Fermi National Accelerator Laboratory

FERMILAB-Pub-91/62-E
[E672/706]

Properties of J/ψ Production in π^--Be and p-Be Collisions at 530 GeV/c

The E672/706 Collaboration
Fermi National Accelerator Laboratory
P.O. Box 500
Batavia, Illinois 60510

March 1991

Operated by Universities Research Association Inc. under contract with the United States Department of Energy

PROPERTIES OF J/ψ PRODUCTION IN π^-–Be AND p–Be COLLISIONS AT 530 GeV/c

V. Abramov, Yu. Antipov, B. Baldin, S. Denisov, V. Glebov,

Yu. Gorin, V. Koreshev, A. Petrukhin, V. Sirotenko, R. Sulyaev

Institute for High Energy Physics, Serpukhov, USSR

R. Gomez

California Institute of Technology, Pasadena, CA 91125

J. Krider

Fermilab, Batavia, IL 60510

H. Goldberg, R. Jesik, S. Margulies, J. Solomon

University of Illinois at Chicago, Chicago, IL 60680

R. Crittenden, K. De, A. Dzierba, A. Gribushin, S. Kartik, R. Li,

S. Markham, T. Marshall, J. Martin, A. Ostrovidov, N. Sinev,

P. Smith, T. Sulanke, K. Welch, A. Zieminski

Indiana University, Bloomington, IN 47405

C. Davis

University of Louisville, Louisville, KY 40292

L. Dauwe

University of Michigan at Flint, Flint, MI 48502

B. Choudhary, V. Kapoor

University of Delhi, New Delhi, India

D. Brown, C. Bromberg, J. Huston, R. Miller

Michigan State University, East Lansing, MI 48824

C. Yosef

Northeastern University, Boston, MA 02115

S. Easo, K. Hartman, B.Y. Oh, W. Toothacker, J. Whitmore

Pennsylvania State University, University Park, PA 16802

E. Engels Jr., S. Mani, P. Shepard, P. Weerasundra

University of Pittsburg, Pittsburg, PA 15260

Fermilab E672 and E706 Collaborations

ABSTRACT

Total and differential cross sections for J/ψ production were measured in the Feynman x region $0.1 \leq x_F \leq 0.8$ with 530 GeV/c proton and π^- beams incident on a beryllium target. We have compared the p_T and x_F distributions with those obtained at lower beam energies and found that the average p_T of J/ψ particles slowly increases with center-of-mass energy, whereas the x_F distribution becomes more centralized. We also found that J/ψs are produced more centrally by protons than by pions. There is similarity, between incident protons and pions, in the properties of the particles, also measured in this experiment, produced in association with J/ψs. We observe the same average charge multiplicities and average forward charges for the proton and pion data. Therefore, we argue that similar mechanisms dominate J/ψ production by these particles and that the differences in the J/ψ Feynman x distributions reflect differences in the proton and pion gluon structure functions. We have also found that the relative production rate of J/ψs and continuum muon pairs does not change with event inelasticity, contrary to the findings of a heavy-ion collision experiment.

1. Introduction

Studies of inclusive hadronic production of J/ψ mesons yield information on a variety of physics topics, and so are of considerable interest. For example, the total and differential cross sections for J/ψ production provide valuable tests of QCD as well as information on hadron structure functions. As gluon fusion is expected to dominate J/ψ production by proton beams,[1,2] the observed cross sections depend on the gluon structure function of the nucleon. For pion beams, a contribution from quark-antiquark annihilations is also expected. The analysis of particles produced in association with J/ψs can thus shed light on the relative contribution of these two mechanisms for pions. In addition, the fraction of J/ψs resulting from radiative decays of charmonium states represents a stringent test of QCD.[3,4]

The A-dependence of J/ψ production is related to the propagation of colored objects through nuclear matter.[5,6] This dependence is also relevant for studies of quark–gluon plasma (QGP). For example, the suppression of J/ψ production has been suggested as the signature of the onset of QGP in nucleus–nucleus collisions.[7] In order to understand this recently observed effect,[8] it is important to first see if suppression occurs in p–nucleus or π^-–nucleus collisions when studied as a function of event inelasticity. Finally, events in which a J/ψ emerges from a secondary decay vertex are uniquely tagged as involving production of a b quark.

This paper describes results from Fermilab E672, a Tevatron fixed-target experiment, which has a potential to address all the topics listed above. The experiment studies hadronic processes yielding high-mass dimuons and

associated particles obtained from proton and pion beams incident on nuclear targets.

In a previous publication[9] we reported results on the A-dependence of J/ψ production in π^-–nucleus collisions. There, we found the exponent α in the cross section parameterization $\sigma(\pi^- \mathrm{A} \rightarrow J/\psi + \mathrm{X}) = \sigma_o \cdot \mathrm{A}^\alpha$ for π^- interacting with a nuclear target of atomic weight A to be $\alpha = 0.85 \pm 0.06$, implying a decreasing effectiveness of J/ψ production with increasing A.

In this paper we investigate the total and differential cross sections for J/ψ production in the Feynman x region $0.1 \leq x_F \leq 0.8$ for proton and π^- beams of 530 GeV/c incident on beryllium. We also analyze the J/ψ production rate as a function of the global properties of the entire event. Here, we concentrate on the energy dependence and beam-particle-type dependence of J/ψ production, on similarities and differences between events produced by protons and pions, and on how the rate depends on the inelasticity of the collision.

Inclusive hadroproduction of J/ψ mesons has been studied in previous experiments up to a center-of-mass energy, $\sqrt{s}$, of 19 GeV for pion beams[10–19] and of 63 GeV for protons.[20–34] This experiment was performed at $\sqrt{s} =$ 31.5 GeV, the highest pion energy to date. The experiment also records information on the associated particles produced, a feature rarely present in previous experiments.[35–38]

This paper is organized as follows: Section 2 describes the apparatus; Section 3 describes the data base and reconstruction of muon tracks. The total and differential cross sections are presented, respectively, in Sections 4 and 5, and are compared with the results of previous experiments. We also

compare our results with a range of predictions for the pion gluon structure function. The general properties of J/ψ events obtained with proton and pion beams are summarized in Section 6. The dependence of the J/ψ production rate on the inelasticity of an event is presented in Section 7. Finally, our conclusions are summarized in Section 8.

2. Apparatus

Fermilab E672 is designed to study dimuon production in an open-geometry configuration. The experiment shares the Fermilab Meson West beamline with E706, an experiment designed to study production of direct photons. The combined apparatus is shown in Fig. 1. The E672 dimuon detector consists of a toroid magnet, proportional wire chambers, and scintillation hodoscopes. The E706 detector contains a liquid argon calorimeter (LAC), a charged-particle spectrometer including silicon-strip detectors (SSDs) and proportional wire chambers (PWCs), and a forward calorimeter.[39] The outputs of all detectors are available to both experiments and this paper reports on data collected in this mode. Our previous publication[9] employed initial data collected with the E672 detector alone before the E706 apparatus became fully operational. A brief description of the essential elements of the combined E672/E706 apparatus used in the present analysis follows.

The Meson West beam line includes a 42-m long differential Cerenkov counter for tagging beam particles. Adequate π^-/K^- discrimination was available for the negative beam, but only meson/proton differentiation was possible for the positive beam. The negative beam included 98.2% $\pi^-$and 1.8% K^-; protons constituted 92% of the positive beam. A hadron shield

consisting of 4 m of iron was located upstream of the target to reduce background from off-axis hadrons and soft muons. The shield was followed by two scintillator veto walls to reject high energy muons that penetrated the iron.

Incident beam hadrons were defined by three scintillation counters located upstream of the target. A valid beam particle required signals from counters SA and SB, and no signal from hole counter SC. The target consisted of two copper foils each 0.8 mm thick, followed by twenty 2-mm-thick sheets of beryllium separated by 1.6 mm.

The charged-particle spectrometer began with three X-Y modules of SSDs[40] which measured the trajectory of incident beam particles upstream of the target. Downstream of the segmented target were four X-Y SSD modules, used to determine the angles of charged particles emerging from the target and to reconstruct interaction and secondary vertices. All SSDs had strips of 50 μm pitch.

A dipole magnet, with tapered aperture, imparting a p_T impulse of 450 MeV/c, was located downstream of the SSD system. Four proportional wire chamber modules followed the magnet. Each module contained wire planes to provide X, Y, U and V measurements. (The U coordinate was 53° above the horizontal; the V coordinate was 37° below the horizontal.) The wires in each plane had a 2.54 mm pitch. A circular area of approximately 10 cm^2 in the center of each plane had reduced sensitivity to provide protection against noninteracting beam particles.

Interactions were detected by a pair of scintillation counters located before the dipole magnet and another pair after the magnet. An interaction

was defined as a signal from any of these counters in coincidence with a valid beam particle. The interaction rate was always less than 0.5 MHz.

Momentum measurements for charged secondaries employed the SSD system, the dipole magnet, and the PWCs. The momentum resolution of the magnetic spectrometer was $\Delta p/p = 0.07\%\ p$. Measurements for high momentum muons which penetrated the muon detector (see below) were improved beyond this value by also using the bend angle in the toroid.

A liquid argon calorimeter[41] was located downstream of the magnetic spectrometer. The LAC contained both electromagnetic and hadronic sections. The outer radius of the electromagnetic section was 1.65 m; the inner radius was 20 cm, corresponding to a helium-gas-filled pipe along the axis of the LAC used to reduce interactions from beam particles. The total LAC material corresponded to six absorption lengths. Approximately 70% of the muons recorded in the muon detector passed through the axial beam pipe. Information from the LAC was not used in the analysis presented here.

Downstream of the LAC was an iron/scintillator forward calorimeter subtending the acceptance region corresponding to the axial beam pipe in the LAC. This calorimeter had a transverse area of 1 m×1 m with a 3 cm diameter axial beam hole and was ten absorption lengths deep.

The E672 dimuon detector, shown in detail in Fig. 2, began 21 m downstream of the target and extended for 15 m. The detector contained, in sequence, three planes (X, Y, U) of PWCs (the D station), a beam dump consisting of tungsten and steel imbedded in concrete, an iron toroid magnet producing an average p_T impulse of 1.3 GeV/c, and four more PWCs (μ_1 through μ_4), each with three planes (X, U, V). In the PWCs the U and V co-

ordinates were at angles of 45° above and below the horizontal, respectively. The four μ PWCs were separated by iron and concrete shielding. Two hodoscope planes (H1 and H2), each made of sixteen sector-shaped scintillation counters, were located in this region with H1 following μ_2 and H2 following μ_4. The acceptance of the muon spectrometer was reduced somewhat by tapered axial holes, starting at 13 cm and ending at 20 cm in radius, in the toroid magnet, muon chambers, and scintillator hodoscopes. The hole in the toroid was filled with lead absorber. The outer radius of the μ chambers and hodoscopes was 135 cm.

The material in the LAC, forward calorimeter, beam dump, toroid, and concrete shielded PWC stations, μ_1 - μ_4, and hodoscope planes, H1 and H2, from hadrons produced in interactions at the target. Muons produced at the target required about 15 GeV of energy to penetrate this material, and particles reaching the hodoscopes were assumed to be muons. Two or more hits in each of H1 and H2 were required for a pretrigger;[42] the average multiplicity was 2.1. In addition to the dimuon detector, information from the veto walls was used as part of the pretrigger requirement. The pretrigger rate for π-Be interactions at 530 GeV/c was 1.3×10^{-4} per interaction. This rate was increased by a factor of 2.5 when the veto walls were not included in the pretrigger. These rates are higher than those reported in our previous publication,[9] the difference resulting from the LAC being centered on the beam instead of blocking it as before, and because of looser beam halo rejection.

The final trigger was formed by a dimuon trigger processor (DMTP), which reconstructed space points in PWCs μ_1 and μ_4, formed muon tracks,

measured their momenta from the estimated bend in the toroid (assuming that the tracks originated in the target), and calculated the dimuon invariant mass. A trigger resulted if any of the dimuon masses, calculated assuming massless muons, was above a preset threshold. A mass threshold of 0.2 GeV/c^2 resulted in a trigger rate of 5×10^{-5} per interaction. The rate could be decreased by a factor of two by increasing the threshold to 1.0 GeV/c^2. The average DMTP processing time was 10 μs, which includes 5 μs spent on decoding the muon chamber data. The combined efficiency of the chambers and the DMTP algorithm was 86% for dimuon events, with half of the losses attributed to "noisy" events where too many hits were recorded. The DMTP mass resolution for the J/ψ was measured to be 550 MeV, consistent with Monte Carlo calculations.

3. Data analysis

Approximately 2×10^6 triggers were recorded, yielding about 10^5 events with a reconstructed dimuon combination. The integrated luminosity per nucleon corresponds approximately to 0.7 pb^{-1} each for incident protons and π^-. Data were collected over a one-month running period.

The sample of events used was selected on the basis of several requirements. The first set of cuts selected dimuon events based on information from the muon detector only. These cuts were as follows:

1. A requirement that muon tracks have spatially correlated hits in the hodoscope planes.
2. Rejection of tracks passing through the lead absorber filling the axial hole of the toroid.

3. A demand that the plane of the beam axis and muon trajectory upstream the toroid be coplanar with that of the beam axis and muon trajectory after the toroid.

These cuts reduced the original sample by a factor of five.

Next, tracks in the muon detector were linked to tracks reconstructed in the charged-particle spectrometer PWCs and SSDs. In this procedure, roads formed around muon trajectories were projected to the PWCs (over a distance of 25 m), and a pattern-recognition algorithm was applied to provide a list of PWC track candidates having at least 12 hits out of a possible 16. An overall χ^2 cut, which considered multiple scattering in the equivalent of 7 m of iron separating the muon chambers and spectrometer PWCs, produced a reduced list of linked track candidates. Halo muon tracks were discarded at this stage. The surviving tracks were then combined with SSD tracks. The new fit included a requirement of consistency of the track momentum as measured with the dipole and toroid magnets. The final fit included an interaction vertex position, determined by the beam particle and other secondaries observed in the event. Multiple vertices were allowed in the fit. The momentum of a track that failed to link with an SSD track was determined from its spectrometer PWC trajectory and vertex position.

After this process a new set of cuts was applied to the data:

1. Only tracks with an SSD link and with χ^2 per degree of freedom less than 2 were kept.

2. Only events with muons orginating from the same vertex were kept.

3. Events with primary vertices outside the Be target volume were dis-

carded.

4. Beam Cerenkov counter information was used to reject events initiated by pions in the positive beam sample and by kaons in the negative beam sample.

5. Only dimuons in the kinematic range $0.1 \leq x_F \leq 0.8$ were accepted.

The effects of the cuts on the data are shown in Table 1. The dimuon mass distributions obtained with incident protons are shown in Fig. 3. The histogram corresponds to unlike-sign muon pairs, and the dotted curve to like-sign pairs. The latter distribution shows no structure, while the former exhibits clear peaks corresponding to production of the ρ/ω, ϕ, and J/ψ vector mesons. Production of the ρ/ω and ϕ will be the subject of a forthcoming publication. In this paper we concentrate on the J/ψ mass region.

The experimental acceptance and efficiency of track reconstruction were estimated by generating 2×10^5 Monte Carlo events. J/ψ mesons were generated with p_T and x_F distributions observed in previous experiments, and were embedded into minimum-bias events possessing multiplicities and particle momenta generated according a longitudinal phase space model. The response of the E672/E706 spectrometer was simulated using GEANT. The simulation included the deadened areas of the PWCs and used measured efficiencies of the SSDs and PWCs. Monte Carlo events which fulfilled the experiment's pretrigger requirements were then processed through a DMTP emulator and the off-line reconstruction program. Finally, the combined acceptance/efficiency was calculated in x_F and p_T bins.

4. Total J/ψ production cross sections

The event distribution in high $\mu^+\mu^-$ mass region, for $0.1 \leq x_F \leq 0.8$, is shown in Fig. 4a and 4b for incident protons and π^-, respectively. The measured J/ψ mass resolutions, rms widths of 75 MeV/c^2 (Fig. 4a) and 80 MeV/c^2 (Fig. 4b), are consistent with Monte Carlo expectations. The poorer mass resolution for the pion data is due to the higher energy of dimuons produced with this beam. Defining the J/ψ mass band to be 2.90 GeV/c^2 $< M_{\mu\mu} <$ 3.30 GeV/c^2 yields a total of 253 and 410 events in this region in the proton and pion samples, respectively.

The background in the J/ψ mass band was estimated by fitting a sum of second order polynomial and J/ψ resolution function to the data in the mass region between 2.0 GeV/c^2 and 4.0 GeV/c^2. Backgrounds were obtained separately for each of the two incident beams. The smooth curves in Fig. 4a and 4b represent the background plus the J/ψ Monte Carlo expectations. Subtraction of the background from the data in the J/ψ mass band yielded 230 and 349 J/ψ events for the proton and pion samples, respectively. Thus, background events in the J/ψ mass band represent 9% and 15% of the total samples. We estimate that approximately 40% of the background in the J/ψ mass band is due to Drell-Yan pair production. The remaining background events are mainly due to muons resulting from pion and kaon decays.

The total cross sections were calculated from $\sigma = N_{evts}/(Le_1e_2e_3)$. Here, N_{evts} represents the measured number J/ψs, L is the integrated luminosity, e_1 is a luminosity correction factor, e_2 is an apparatus efficiency factor, and e_3 is a combined acceptance and off-line-reconstruction efficiency factor. The

values of quantities used in the cross section calculations are given in Table 2. Below we explain them in more detail.

The integrated luminosity was calculated from the total number of beam particles incident on the 7.4 g/cm^2 Be target during the live time of the experiment, and using 183 mb and 138 mb for the total inelastic pBe and π^-Be cross sections, respectively.[43]

The luminosity correction factor, e_1, includes:

1. Clean interactions and halo muon rejection. The luminosity was corrected for interactions lost due to a 150 ns-wide veto on beam-halo muons, and for a requirement that no interaction occured within $\pm$ 3 beam buckets of the event (a "clean" interaction). In addition, we demanded that the incident hadron be unaccompanied by another beam particle within $\pm$ 20 ns.

2. Hardware event rejection. Some interactions were lost due to a veto on events with a noisy signal from the LAC.

3. Backscatter. Backscattering from the target could cause signals from the veto walls which would veto the event. The magnitude of this effect was estimated from a sample of the data taken without requiring the veto. The correction is $(5 \pm 2)\%$.

The result of these effects is to produce luminosity correction factors of 0.54 ± 0.03 and 0.60 ± 0.03 for the proton and pion induced data, respectively.

The apparatus efficiency factor, e_2, includes:

1. Pretrigger efficiency. Each counter in hodoscopes H1 and H2 operated

at 94% efficiency. The overall correction factor for detection losses was 24%.

2. DMTP efficiency. "Noisy" events could overfill the DMTP buffer, which has limits of 15 space points per chamber and 15 tracks in PWCs μ_1 - μ_4. These losses amounted to 8% of the events.

The result of these effects is to produce an apparatus efficiency factor of 0.70 ± 0.06.

The acceptance and off-line reconstruction efficiency factor, e_3, includes the following effects, some discussed in more detail in Section 3:

1. Chamber efficiencies. The per-plane efficiencies were 93%, 94%, and 99% for the SSDs, spectrometer PWCs, and muon-detector PWCs, respectively. These effects are included in the Monte Carlo calculations used to estimate the off-line reconstruction efficiency.

2. Dimuon selection efficiency. The criteria used to select dimuon event candidates from the total data sample produced a 6% loss of J/ψ events.

3. Track linking efficiency. Linking muon tracks from the muon detector to the spectrometer PWCs and SSDs resulted in a reconstruction efficiency of 72%.

4. Track quality cut efficiency. Requiring that reconstructed tracks have certain quality properties produced a 15% loss.

5. Vertex cut efficiency. Requiring that events have reconstructed vertices within the target volume yielded a 7% loss.

6. Integrated acceptance. The integrated geometrical acceptance in the

kinematic region $0.1 \leq x_F \leq 0.8$ was estimated by applying two-dimensional x_F and p_T acceptance curves to the data.

The result of these effects produces off-line reconstruction efficiency factors of 0.17 ± 0.03 and 0.19 ± 0.03 for incident protons and pions, respectively.

After applying the corrections described above, the J/ψ cross section per nucleon, in the region $0.1 \leq x_F \leq 0.8$, was found to equal (4.3 ± 0.9) nb and (7.3 ± 1.6) nb for pBe and π^- Be interactions, respectively. These values include the branching ratio for the decay $J/\psi \longrightarrow \mu^+\mu^-$.

For comparison with other experiments, where the data cover larger kinematic regions, our cross sections were corrected to extend to the region x_F=0 by extrapolating our x_F distributions, discussed in the next section (Eq.(4)). This procedure yielded correction factors of 1.23 ± 0.03 and 1.9 ± 0.1 for the proton and π^- samples, respectively. The corresponding per nucleon cross sections are then (7.7 ± 1.7) nb for pBe, and (9.0 ± 2.0) nb for π^- Be.

The dependence of the per-nucleon J/ψ cross section on $\sqrt{s}$, for $x_F \geq 0$, is shown in Fig. 5a and 5b. The effect of different targets used by various experiments was taken into account by normalizing all data to beryllium assuming an $A^{0.9}$ nuclear mass number dependence.[9,28] As can be seen, our results agree well with previous values, including the cross sections we presented previously.[9] The curves in Figs. 5 represent parameterizations of the J/ψ cross section using the simple empirical formula

$$\sigma = \sigma_0(1 - M_\psi/\sqrt{s})^n. \qquad (1)$$

The values of the parameters σ_0 and n resulting from fits to the data shown are given in Table 3.

5. Differential cross sections for J/ψ production

We have analyzed J/ψ differential distributions as functions of several variables. In this experiment it was impossible to distinguish J/ψs produced directly from those resulting from ψ' or χ decays. Thus no corrections were made for indirect J/ψ production.

In this section we present differential distributions along with empirical fits using simple mathematical forms. The resulting parameters that characterize the data are summarized in Table 4. In addition, we examine the dependence of these parameters on $\sqrt{s}$ by considering results from previous experiments in addition to our own. This dependence is also fitted with simple empirical expressions. The results of these parameterizations are summarized in Table 3.

(a) Longitudinal momentum variables

The dependence on x_F of the per-nucleon J/ψ cross section, corrected for the apparatus acceptance and with background subtracted, is shown in Fig. 6a and 6b for incident protons and π^-, respectively. The acceptance (not shown) is largest in the region $0.1 \leq x_F \leq 0.8$, for which the integrated acceptance was approximately 40%. The background was determined by constructing x_F distributions for $\mu^+\mu^-$ pairs from regions adjacent to the J/ψ mass band and performing appropriate normalization.

The dashed curves in Fig. 6a. and 6b. represent fits to the form

$$dN/dx_F \sim (1 - |x_F - x_0|)^c \qquad (2)$$

with $x_0 = 0.0$ for the proton- induced data and $x_0 = 0.18$ for the π^--induced

data. The corresponding values of c are 5.13 ± 0.46 and 3.49 ± 0.33.

The variation of the parameter c with $\sqrt{s}$ is shown in Fig. 7a for the proton beam and in Fig. 7b for the π^- beam. Data in these figures from other experiments were obtained from fits to the form given in Eq. (2) when not so parameterized by the authors themselves. The solid curves represent fits to the expression

$$c = a/(1 + b/\sqrt{s}). \tag{3}$$

The values of parameters a and b were found to be 4.11 ± 0.26 and 10.2 ± 1.5, respectively, for the π^- data. The value of c is relatively constant over the range of $\sqrt{s}$ for the π^- data. For the proton data, c increases significantly with energy, indicating a trend to more central J/ψ production.

The solid curves in Fig. 6a and 6b represent fits to the forms

$$dN/dx_F \sim (1 - x_1)^\kappa (1 - x_2)^\kappa / (x_1 + x_2) \tag{4}$$

and

$$dN/dx_F \sim (1 - x_1)^\kappa (1 - x_2)^{2+\kappa} / (x_1 + x_2) \times x_1^a, \tag{5}$$

respectively.[44] Here, x_1 represents the beam parton relative momentum and x_2 the target parton relative momentum. If gluon fusion is the dominant mechanism responsible for the J/ψ production with incident protons then the expected values of the parameter κ are 5 for J/ψs produced predominantly through χ states decays, and 6 for direct J/ψ production. For incident pions the gluon fusion mechanism predicts κ to be 3 and 4 for the indirect and direct J/ψ production, respectively. The qq annihilation mechanism predicts

values of κ smaller by one unit. We find values of κ equal to 4.1 ± 0.5 and 3.4 ± 0.7 for the proton and π^- induced events, respectively. Our data are not precise enough to differentiate between the parameterizations of Eq. (2) and Eqs. (4) or (5). The parameter κ for the π^- induced reactions does not change much with $\sqrt{s}$, as shown in Fig. 7c.

Finally, Figs. 6c and 6d compare our results with predictions of a simple model including first-order gg and $q\bar{q}$ annihilation diagrams and assuming decolorization by soft gluon emission[2]. This model has been used previously to determine gluon structure functions within a pion.[2,17] Our statistics are insufficient for an independent gluon structure-function determination. Instead formulas and parameters from Ref. 2 are used, except for the pion gluon structure function for which we vary the exponent N in the parameterization $xG(x) = (1-x)^N$. Figure 6c compares the x_F distributions for the pion data with the model predictions for N=1.9. Also shown are the individual contributions from gluon fusion (dashed curve) and qq annihilation (dotted curve). Gluon fusion dominates the spectrum for $x_F \leq 0.8$. Figure 6d shows the ratio of the x_F distributions for the proton and pion induced data. The pion spectrum is much harder than those for protons. If gluon fusion is responsible for the J/ψ production for both beams, as indicated in Fig. 6c and as we also try to demonstrate in the next section, then the ratio in Fig. 6d predominantly reflects the difference in the gluon structure function for pions and protons. Since the proton and pion induced data were collected with the same apparatus, the ratio presented in Fig. 6d should be free of many systematic errors. The model predictions shown in Fig. 6d are for values of N (for pions) equal to 1.0 (dashed curve), 1.9 (topsolid

curve) and 3.0 (dotted curve). Our data are consistent with N = 2.0± 0.5, in agreement with findings of Refs. 12 and 17.

(b) Transverse momentum variables

The per-nucleon transverse-momentum squared distributions, corrected for acceptance and with background subtracted, are shown in Fig. 8a and 8b for incident protons and π^-, respectively. The p_T acceptance of the apparatus was essentially flat up to 5 GeV/c. As can be seen, there is little difference in the ${p_T}^2$ distributions obtained with incident protons and incident π^-. The average values of transverse momentum, $<p_T>$, are (1.06 ± 0.05) GeV/c and (1.13 ± 0.04) GeV/c, for incident protons and pions, respectively.

The average values of transverse momentum, $<p_T>$, are shown as functions of $\sqrt{s}$ in Figs. 9. The $<p_T>$ grows linearly with the c.m. energy in agreement with the QCD expectations.[45]

6. Associated charged particle production

The properties of the hadrons produced in association with J/ψs should shed light on the mechanism by which J/ψ mesons are produced in hadronic interactions. Among these properties are the multiplicities and charges of the forward-going hadronic system (i.e., hadrons with positive x_F). In the hadronic production of a J/ψ at $x_F > 0.1$, a parton from the beam particle interacts with a parton from the target nucleon. The spectator partons from the beam particle then fragment into hadrons. If the dominant mechanism is gluon fusion, then the net charge of the beam jet from the spectator partons should equal that of the incident beam particle. On the other hand, quark-antiquark annihilation, expected to contribute to J/ψ production by incident

π^-, will primarily involve $u\bar{u}$ pairs and should, naively, leave noninteracting partons with a net charge of -1/3. More refined calculations, which include the lower probability process of s quarks participating in the fragmentation, predict this number to be -0.44. The charge of the beam spectator partons should manifest itself as an average charge, $< Q >_f$, of hadrons produced forward in the c.m. frame. However, there are other effects which may influence the measured forward charge. They include leakage of slow hadrons through the border between the beam and target fragmentation regions, resonance production and nuclear target effects. On the other hand, it is reasonable to assume that these effects are similar for proton and π^- induced reactions. Therefore, the difference in $< Q >_f$ for the proton and π^- data may be used to determine the relative contributions of gluon fusion and $q\bar{q}$ annihilations to J/ψ hadroproduction.

Charged secondaries accompanying a J/ψ were reconstructed using information from the spectrometer PWCs and SSDs. (Muons were removed from the list of reconstructed particles). To estimate the reliability of our off-line track reconstruction program and the effects of reconstructing spurious tracks, a Monte Carlo program which included detector plane efficiencies and desensitized areas was employed. Based on these studies, each track was assigned a weight that depended on the event multiplicity, track momentum, and polar angle. These weights did not differ from unity by more than 10%. We estimate that the overall uncertainty in track multiplicity is less than 1.0. The relative uncertaintity between either the proton and π^- data or between different dimuon mass bins is less than 0.2.

The dependence of $< N_{ch} >_f$, the average charge multiplicity in the

forward region, on dimuon mass is shown in Fig.10 for both beam particle types. The value of $< N_{ch} >_f$ decreases slowly with dimuon mass, with a smooth transition between the J/ψ mass band (2.90 GeV/c^2 $<M_{\mu\mu}<$ 3.3 GeV/c^2) and the adjacent region. The same trend was observed in Ref. 36. Within the uncertainties, the values of $< N_{ch} >_f$ are identical for proton and π^- induced events for $M_{\mu\mu}$ >2.7 GeV/c^2.

More variation is found in the dependence of $< N_{ch} >_f$ on x_F of the dimuon pair for the pion data, shown in Fig. 11. The figure shows data for the J/ψ region and for the adjacent mass band. The values of $< N_{ch} >_f$ for both J/ψ events and non-resonant dimuon pairs decrease with x_F of the dimuon. The same effect can not be excluded for the proton data, also shown in Fig. 11. However, there is an indication that in the x_F >0.5 region values of $< N_{ch} >_f$ are lower for π^- than for proton induced events.

Figures 12 display $< N_{ch} >_f$ as a function of p_T of the dimuon pair with data shown for the J/ψ region and for the adjacent mass band. The value of $< N_{ch} >_f$ increases somewhat with p_T for both mass regions. No significant differences are observed between data collected with incident proton and π^- beams for the J/ψ events.

Next, the average forward charge distributions are investigated. The forward charge sum, Q_f, is formed by algebraically adding the charges of all hadrons with positive x_F. The dependence of $< Q >_f$ on dimuon mass is shown in Fig. 13a. The dependence is not strong, and the value of $< Q >_f$ for J/ψ events is equal to 0.56±0.08 for proton induced events and -0.61±0.06 for π^- events. The π^- result is close to those obtained by other experiments.[38] There is no evidence for the dependence of $< Q >_f$ on

the dimuon x_F and p_T variables, as may be seen from Figs. 13b and 13c, respectively. With incident π^-, the gluon fusion process is expected to dominate J/ψ production at small values of x_F. Therefore, $< Q >_f$ is expected to become less negative as x_F of the J/ψ increases. The data show no evidence for such an effect, in agreement with previous observations.[38]

We conclude that the basic properties of the particles accompanying a J/ψ are similar for the proton and pion induced data, therefore supporting the conjecture that gluon fusion is the dominant mechanism responsible for J/ψ production in both cases.

7. J/ψ production-rate dependence on event inelasticity

In this section we analyze the dependence of the yield of J/ψs relative to muon pairs produced in the mass continuum as a function of the inelasticity of the collision. Previous studies of oxygen-uranium reactions at 200 GeV/nucleon indicated a strong suppression of the relative J/ψ yield for collisions in which large transverse energy was observed.[8] This observation was consistent with model predictions for quark-gluon plasma formation. However, the authors of Ref.8 could not exclude alternative explanations of the suppression by hadronic mechanisms.[46] Since, the range of transverse energies per nucleon available in this experiment approximately corresponds to that of Ref. 8, it is interesting to apply their analysis to our data.

In order to increase the statistics for this study, the data taken with the negative and positive beams were combined. The variable of interest is E_T, the transverse energy of the event, as a scalar sum of transverse momenta of all observed charged particles. The ratio of N_ψ, the number

of events in the J/ψ mass band, to N_{adj} the number in the adjacent band 2.5 GeV/c^2 < $M_{\mu\mu}$ < 2.8 GeV/c^2, is shown in Fig. 14 as a function of E_T. There is no indication for J/ψ suppression at large E_T. Several additional methods, with and without background subtraction, were applied to estimate the J/ψ to continuum ratio. All gave results consistent with those shown in Fig. 14. Thus our data confirm the statement made in Ref. 8, that the J/ψ suppression seen in heavy-ion collisions is not observed in hadron-nucleus interactions.

8. Conclusions

We have studied the production of J/ψs by 530 GeV/c negative pions and protons incident on a beryllium target. Total and differential cross sections in the forward region ($0.1 \leq x_F \leq 0.8$) were measured. Upon comparing the observed p_T and x_F distributions with those obtained at lower beam energies, it was found that the average p_T of J/ψ particles slowly increases with $\sqrt{s}$, whereas the x_F distributions slowly become more centralized. It was also found that J/ψs are produced more centrally with incident protons than with pions. The experiment also detected charged particles produced in association with J/ψs. The properties of the associated particles were basically similar for proton and π^- induced events. We observed the same average charge multiplicities and absolute average forward charges for both. Therefore, we argue that similar mechanisms dominate J/ψ production by protons and pions, and that the differences in the J/ψ Feynman x distributions reflect differences in the proton and pion gluon structure functions. We have also found that the relative rate of J/ψs to continuum pair production does not change with the inelasticity of events, contrary to findings in

heavy-ion collisions.

Acknowledgments

We thank the staffs of all the participating institutions, especially the assistance of Fermilab and the Institute for High Energy Physics (IHEP) at Serpukhov. We acknowledge a very fruitful and friendly cooperation between E672 and E706 Collaborations. This research was supported in parts by the Department of Energy, the National Science Foundation, and the USSR State Committee for Utilization of Atomic Energy.

REFERENCES

1. C. E. Carlson and R. Suaya, *Phys. Rev.* **D18**, 760 (1978) ; L. Clavelli et al., *Phys. Rev.* **D32**, 612 (1985) and references therein.

2. V. Barger et al., *Phys. Lett.* **91B**, 253 (1980) and, *Z. Phys.* **C6**, 169 (1980) .

3. Y. Lemoigne et al., *Phys. Lett.* **113B**, 509 (1982) ; S. Hahn et al., *Phys. Rev.* **D30**, 671 (1984) and references therein.

4. R. Bailer and R. Rückl, *Z. Phys.* **C19**, 251 (1983) and references therein.

5. B. Kopeliovich and F. Niedermayer, Dubna preprint, JINR-E2-84-834 (1984) (unpublished) and, *Sov. J. Nucl. Phys.* **42**, 504 (1985) .

6. T. Hoang, *Phys. Rev.* **D39**, 2050 (1989) ; J. Qui, *Nucl. Phys.* **B291**, 746 (1987) ; S. Brodsky and A. Mueller, SLAC preprint, NSF-ITP-88-22 (1988) (unpublished).

7. T. Matsui and H. Satz, *Phys. Lett.* **178B**, 416 (1978) ; J. Milana, *Phys. Rev. Lett.* **62**, 2921 (1989) .

8. C. Baglin et al., *Phys. Lett.* **220B**, 471 (1989) .

9. S. Kartik et al., *Phys. Rev.* **D41**, 1 (1990) .

10. J. Lebritton et al., *Phys. Lett.* **81B**, 397 (1979) and, *Phys. Lett.* **81B**, 401 (1979) .

11. Yu. Bushin et al., *Phys. Lett.* **72B**, 269 (1977) ; R. Dzhelyadin et al., *Nucl. Phys.* **B179**, 189 (1981) .

12. F. Binon et al., *Nucl. Phys.* **B239**, 311 (1984) .

13. M. Corden et al., *Phys. Lett.* **68B**, 96 (1977) ;, *Phys. Lett.* **96B**, 411 (1980) ;, *Phys. Lett.* **98B**, 220 (1980) .

14. Yu. Antipov et al., *Phys. Lett.* **72B**, 278 (1977) and, *Phys. Lett.* **76B**, 235 (1978) .

15. S. Katsanevas et al., *Phys. Rev. Lett.* **60**, 2121 (1988) .

16. S. Tzamarias et al., Fermilab preprint, FERMILAB-Pub-90/63-E (1990).

17. M. Abolins et al., *Z. Phys.* **82B**, 145 (1979) ; J. Badier et al., *Z. Phys.* **C20**, 101 (1983) ; J. McEwen et al., *Phys. Lett.* **121B**, 198 (1983) .

18. J. Branson et al., *Phys. Rev. Lett.* **38**, 1331 (1977) .

19. K. McDonald, Proceedings of the QCD Workshop, St. Croix, V.I., World Scientific, edited by B. Cox, p.57 (1989).

20. A. Bamberger et al., *Nucl. Phys.* **B134**, 1 (1978) .

21. Yu. Antipov et al., *Phys. Lett.* **60B**, 309 (1976) .

22. K. J. Anderson et al., *Phys. Rev. Lett.* **36**, 237 (1976) and, *Phys. Rev. Lett.* **37**, 799 (1976) .

23. K. J. Anderson et al., *Phys. Rev. Lett.* **42**, 944 (1979) .

24. B. Knapp et al., *Phys. Rev. Lett.* **34**, 1044 (1975) .

25. M. Binkley et al., *Phys. Rev. Lett.* **37**, 571 (1976) .

26. H. D. Snyder et al., *Phys. Rev. Lett.* **36**, 1415 (1976) .

27. E. J. Siskind et al., *Phys. Rev.* **D21**, 628 (1980) .

28. D. M. Alde et al., *Phys. Rev. Lett.* **66**, 133 (1991) .

29. E. Nagy et al., *Phys. Lett.* **60B**, 96 (1975) .

30. E. Amaldi et al., *Lett. Nuovo Cim.* **19**, 152 (1977) .

31. A. G. Clark et al., *Nucl. Phys.* **B142**, 29 (1978) .

32. F. W. Busser et al., *Phys. Lett.* **56B**, 482 (1975) .

33. C. Kourkomelis et al., *Phys. Lett.* **91B**, 481 (1980) .

34. J. H. Cobb et al., *Phys. Lett.* **68B**, 101 (1977) .

35. D. Antreasyan et al., *Nucl. Phys.* **B199**, 365 (1985) .

36. D. Antreasyan et al., *Il Nuovo Cim.* **99A**, 595 (1988) .

37. B. Pietrzyk et al., *Phys. Lett.* **113B**, 105 (1982) .

38. H. S. Budd et al., *Phys. Rev.* **D31**, 1132 (1985) .

39. G. Ginther et al., Proceedings of the 1989 Rencontre de Moriond, edited by J. Tran Thanh Van, Editions Frontiers, p.181

40. E. Engels et al., *Nucl. Instr. & Meth.* **A279**, 272 (1989) .

41. F. Lobkowicz et al., *Nucl. Instr. & Meth.* **A235**, 332 (1985) .

42. R. Crittenden et al., *Nucl. Instr. & Meth.* **A270**, 99 (1988) .

43. A.S. Carroll et al., *Phys. Lett.* **80B**, 319 (1979) .

44. V. Kartvielishvili and A.K. Likhoded, *Sov. J. Nucl. Phys.* **39**, 298 (1984) .

45. G. Altarelli, G. Parisi and R. Pettronzio, *Phys. Lett.* **76B**, 351 (1978)

46. A. Cappella et al., preprint LPTHE Orsay 90/02 (1990)

FIGURE CAPTIONS

1) Layout of the E672/E706 apparatus.

2) Layout of the E672 muon spectrometer.

3) Dimuon mass spectra for incident protons. The histogram corresponds to unlike-sign muon pairs, and the dotted curve to like-sign pairs.

4) Opposite-sign dimuon mass spectrum in the J/ψ region for incident (a) protons, (b) π^-. The smooth curves represent the sums of background and the results of a J/ψ Monte Carlo calculation, as described in the text.

5) Total J/ψ cross sections as a function of $\sqrt{s}$ for incident (a) protons, (b) π^-.

6) J/ψ cross section as a function of x_F for incident (a) protons, (b) π^-. The dashed curves represent results fits to the data with the form of Eq. (2). The solid curves represent results of fits using the form of Eqs. (4) and (5). (c) J/ψ cross section as a function of x_F for incident π^-. The solid curve represents predictions of the gluon fusion model of Ref. 2 with N=1.9. The dashed and dotted curves represent contributions of gluon fusion and qq annihilation, respectively. (d) Ratio of the x_F distributions for proton and pion data. Dotted, solid, and dashed curves show predictions of the gluon fusion model of Ref. 2 assuming values of the exponent N of 3, 1.9 and 1.0, respectively, for pions.

7) Dependence of the parameter c (Eq. (2)) on $\sqrt{s}$: (a) protons, (b) π^-. (c) Dependence of the parameter κ (Eq. (5)) on $\sqrt{s}$ for incident pions.

8) Distribution of $p_T{}^2$ for J/ψ events for incident (a) protons, (b) π^-.

9) Dependence of $<p_T>$ on $\sqrt{s}$ for incident (a) protons, (b) π^-.

10) Average forward charge multiplicity as a function of dimuon mass.

11) Average forward charge multiplicity as a function of dimuon x_F for incident (a) protons, (b) π^-.

12) Average forward charge multiplicity as a function of dimuon p_T for incident (a) protons, (b) π^-.

13) Average charge in the forward direction as a function of (a) dimuon mass, (b) dimuon x_F and (c) dimuon p_T for incident protons and π^-.

14) The ratio of the number of events in the J/ψ mass region to that in the adjacent mass region as a function of the transverse energy of all charged particles observed in the event.

Table 1

Reconstructed dimuon events

Requirement	Protons	Pions
MUON-PWC-SSD linked dimuons	34,815	47,251
Primary vertex in Be target	27,913	39,275
Beam Cerenkov rejection	25,415	35,636
$\mu^+\mu^-$ pairs	16,211	21,658
$\chi^2 < 2.0$	12,813	17,314
$0.1 \leq x_F \leq 0.8$	11,780	16,171
2.9 GeV/c^2 < $M_{\mu\mu}$ < 3.3 GeV/c^2	253	410
Number of J/ψ events	230	349

Table 2

J/ψ cross section calculations ($0.1 \leq x_F \leq 0.8$)

Quantity	Protons	Pions
Integrated luminosity / nucleon, pb^{-1}	0.83	0.60
Number of J/ψ events ($0.1 \leq x_F \leq 0.8$)	230	349
LUMINOSITY CORRECTIONS		
Clean interactions	0.88±0.01	0.92±0.01
Halo muon rejection	0.80±0.01	0.76±0.01
Hardware event rejection	0.80±0.01	0.91±0.01
Backscatter	0.95±0.02	0.95±0.02
TOTAL	0.54±0.03	0.60±0.03
APPARATUS CORRECTIONS		
Pretrigger counters	0.76±0.06	0.76±0.06
DMTP	0.92±0.03	0.92±0.03
TOTAL	0.70±0.06	0.70±0.06
OFFLINE CORRECTIONS		
Event preselection	0.94±0.02	0.94±0.02
Muon tracks linking	0.72±0.06	0.72±0.06
Track quality cuts	0.85±0.06	0.85±0.06
Mass cut	0.87±0.03	0.84±0.03
Primary vertex reconstruction	0.93±0.03	0.93±0.03
Geometrical acceptance ($0.1 \leq x_F \leq 0.8$)	0.37±0.03	0.43±0.03
TOTAL	0.17±0.03	0.19±0.03
TOTAL CROSS SECTION ($0.1 \leq x_F \leq 0.8$), nb	4.3±0.9	7.3±1.6
TOTAL CROSS SECTION ($0.1 \leq x_F \leq 0.8$), nb	7.7±1.7	9.0±2.0

Table 3

C.M. energy parameterizations of J/ψ cross sections

Quantity	Formula used	Fitted values of parameters	
		Protons	Pions
Total cross section	$\sigma = \sigma_0(1 - M_\psi/\sqrt{s})^n$	$\sigma_0 = (30.6 \pm 5.0)$ nb/nucl. $n = 12.0 \pm 0.9$	$\sigma_0 = (23.3 \pm 2.6)$ nb/nucl. $n = 7.3 \pm 0.5$
$c(x_F)$	$c = a/(1 + b/\sqrt{s})$	$a = 13.5 \pm 4.5$ $b = (44.9 \pm 21.9)$ GeV	$a = 4.11 \pm 0.28$ $b = (10.2 \pm 1.5)$ GeV
$\kappa(x_F)$	$\kappa = a/(1 + b/\sqrt{s})$		$a = 3.21 \pm 0.36$ $b = (8.6 \pm 2.3)$ GeV
$<p_T>$	$<p_T> = a + b\sqrt{s}$	$a = (0.74 \pm 0.03)$ GeV/c $b = 0.011 \pm 0.001$	$a = (0.73 \pm 0.03)$ GeV/c $b = 0.014 \pm 0.002$

Table 4

Parameters of differential cross sections

Quantity	Protons	Pions
x_0 (assumed)	0.0	0.18
$c\,(x_F)$	5.13 $\pm$ 0.46	3.49 $\pm$ 0.33
$\kappa\,(x_F)$	4.11 $\pm$ 0.50	3.38 $\pm$ 0.71
$<p_T>$, GeV/c	1.06 $\pm$ 0.05	1.13 $\pm$ 0.04
$<p_T{}^2>$, (GeV/c)^2	1.55 $\pm$ 0.11	1.72 $\pm$ 0.10

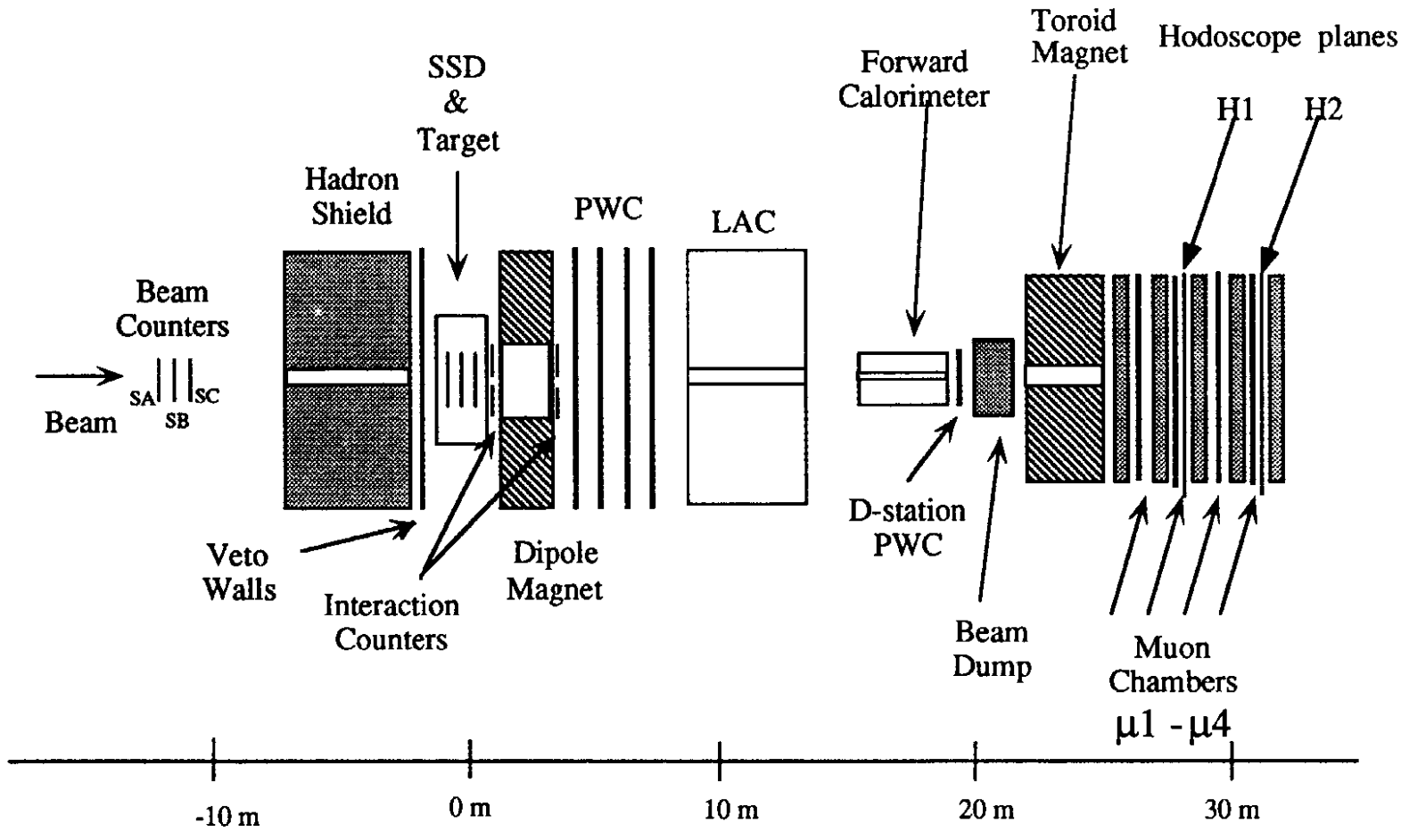
The E672/E706 Apparatus
Toroid Magnet
Hodoscope planes
Forward Calorimeter
SSD & Target
H1
H2
Hadron Shield
PWC
LAC
Beam Counters
SA
SC
SB
Beam
Veto Walls
Interaction Counters
Dipole Magnet
D-station PWC
Beam Dump
Muon Chambers
μ1 - μ4
-10 m
0 m
10 m
20 m
30 m

Fig. 1

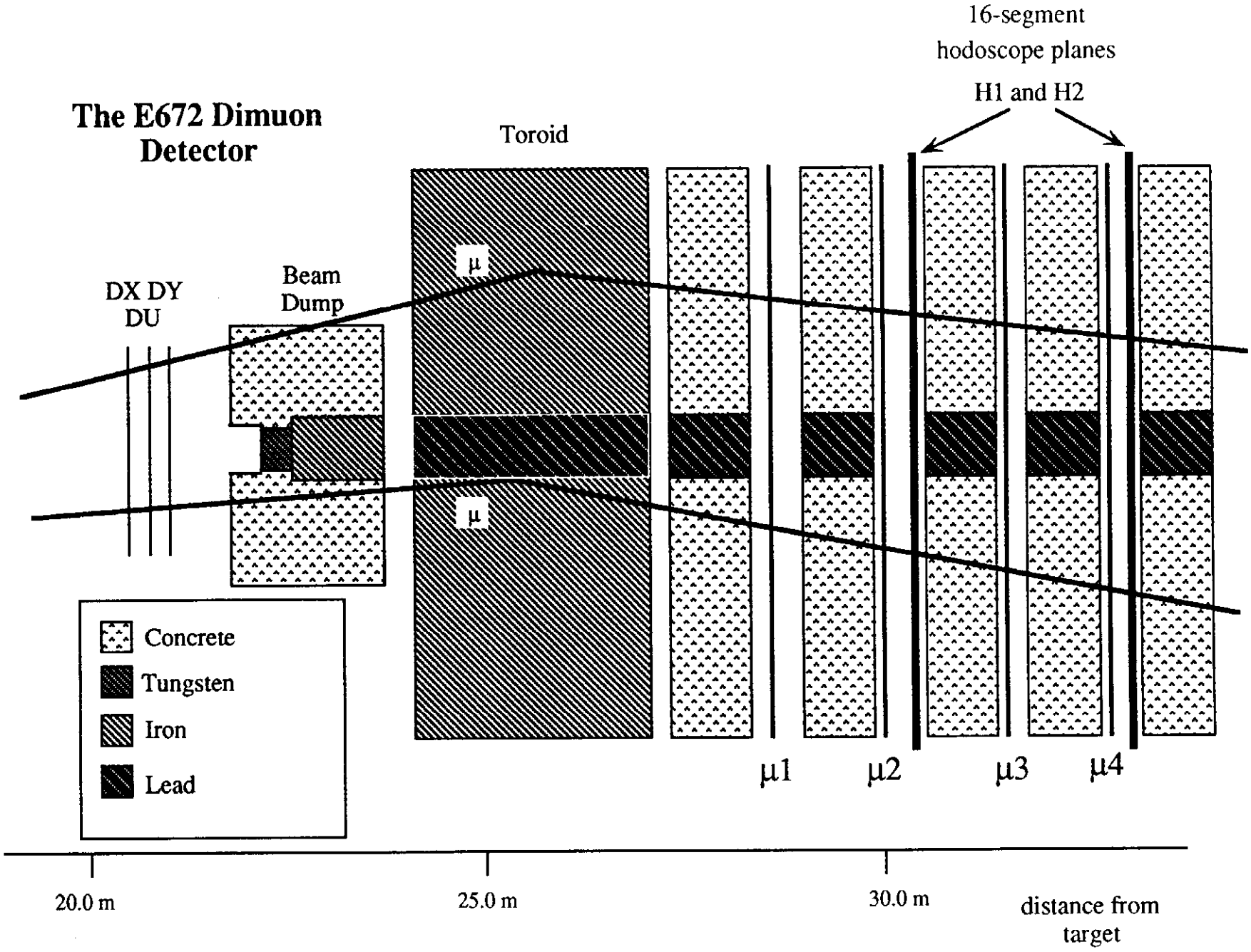
The E672 Dimuon Detector
16-segment hodoscope planes
H1 and H2
Toroid
DX DY DU
Beam Dump
μ
μ
μ1
μ2
μ3
μ4
Concrete
Tungsten
Iron
Lead
20.0 m
25.0 m
30.0 m
distance from target

Fig. 2

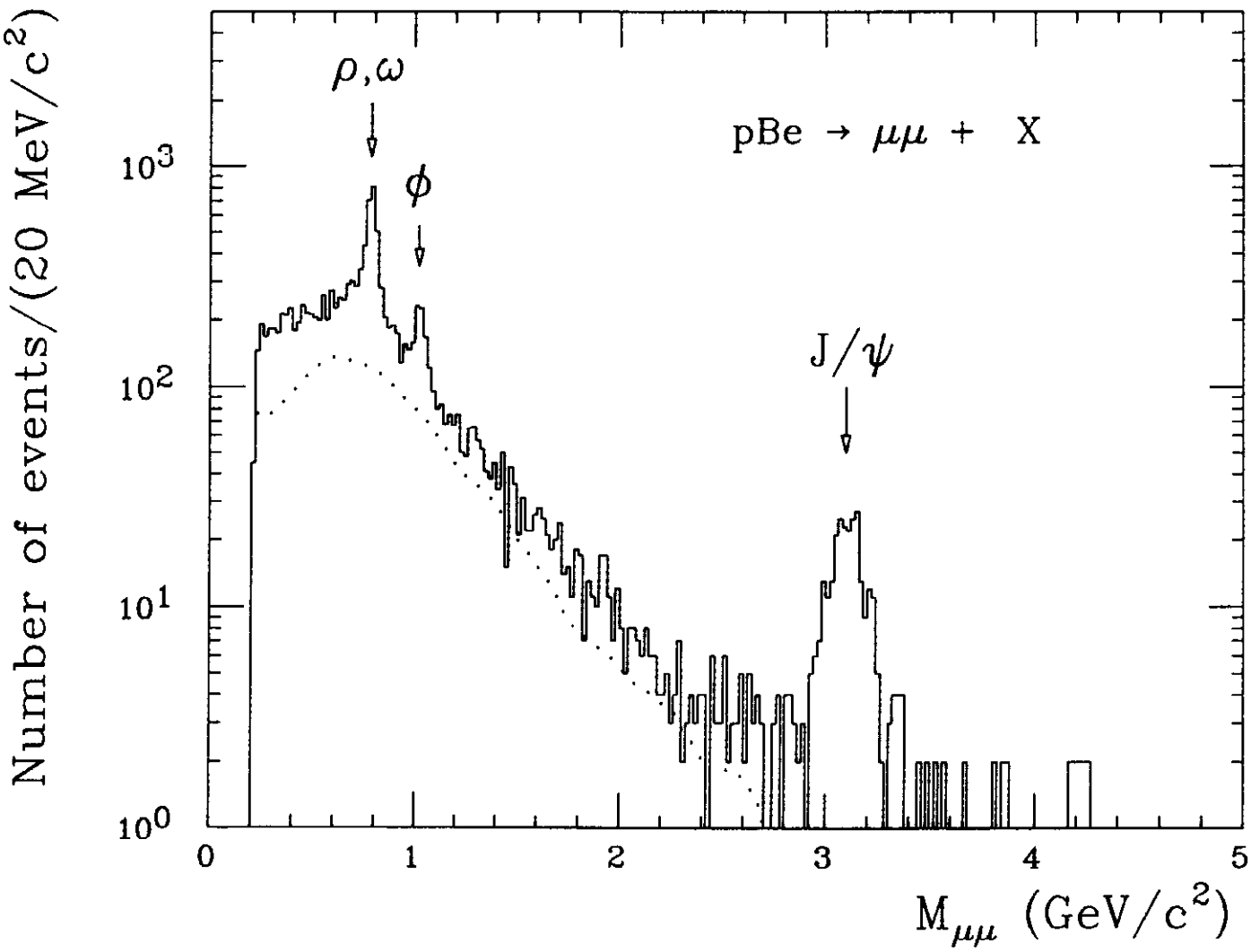
Number of events/(20 MeV/c²)
ρ,ω
φ
J/ψ
pBe → μμ + X
10³
10²
10¹
10⁰
0
1
2
3
4
5
M_μμ (GeV/c²)

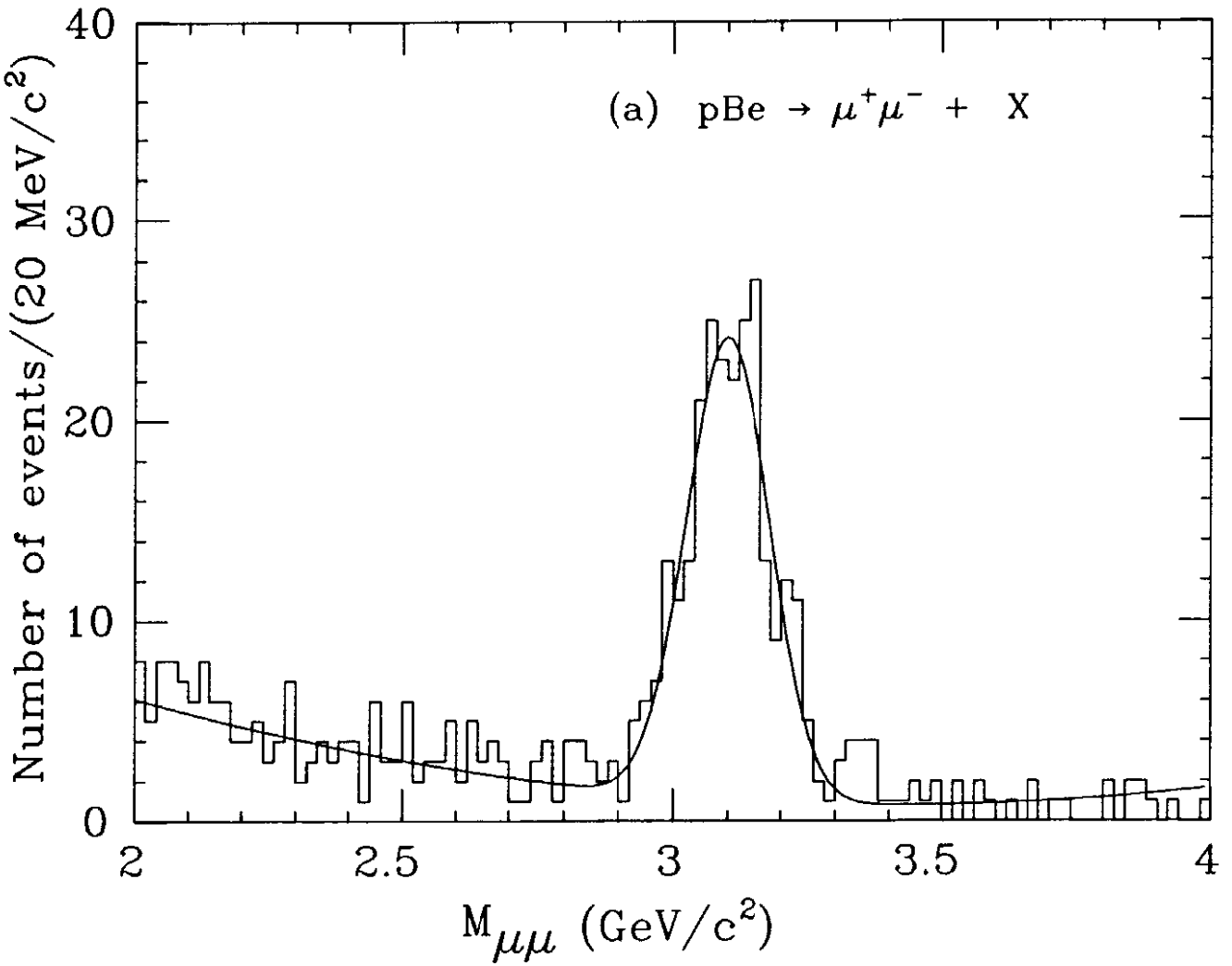
(a) pBe → $\mu^+\mu^-$ + X
Number of events/(20 MeV/c^2)
$M_{\mu\mu}$ (GeV/c^2)
0
10
20
30
40
2
2.5
3
3.5
4

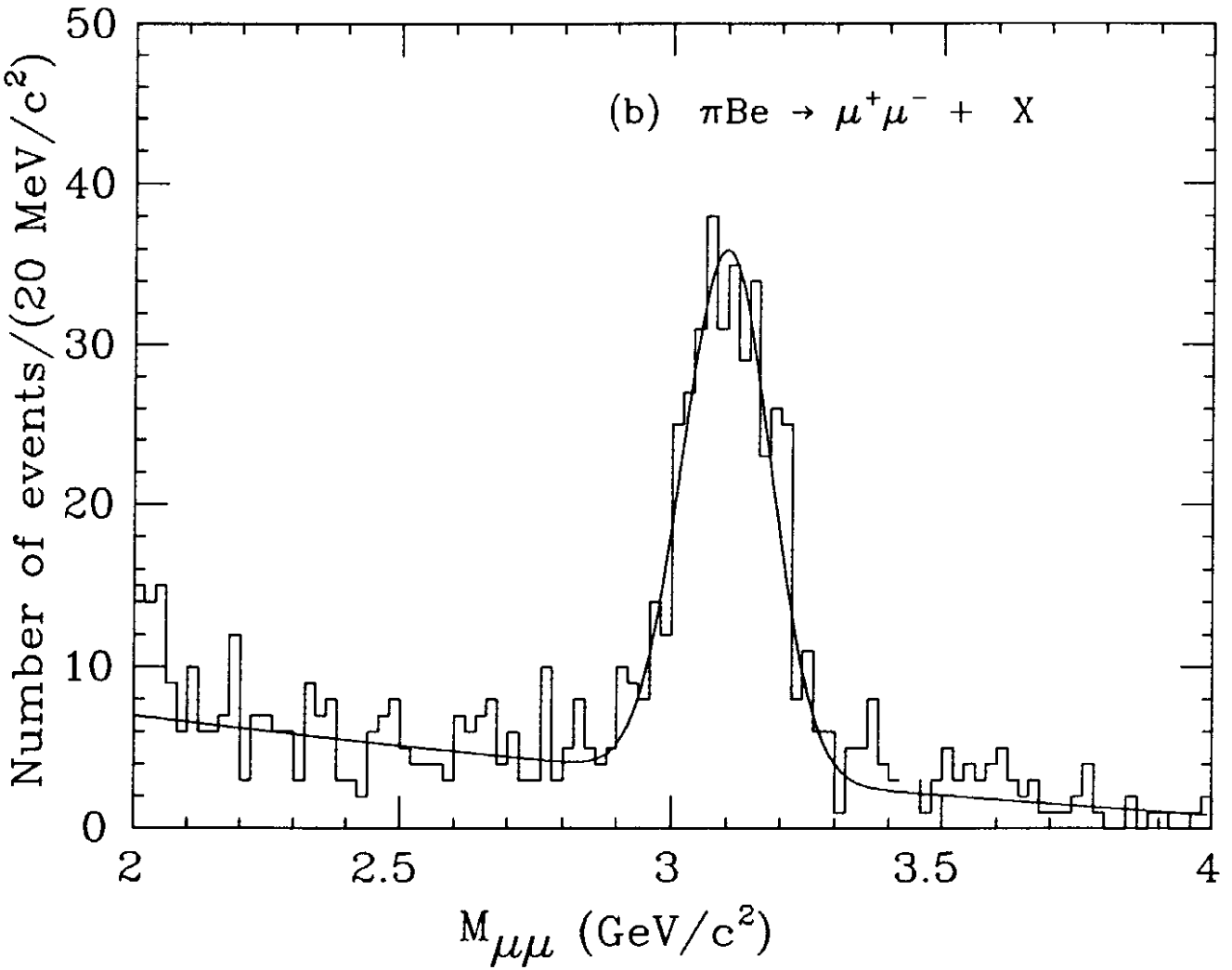
(b) πBe → μ⁺μ⁻ + X
Number of events/(20 MeV/c²)
M_μμ (GeV/c²)
0
10
20
30
40
50
2
2.5
3
3.5
4

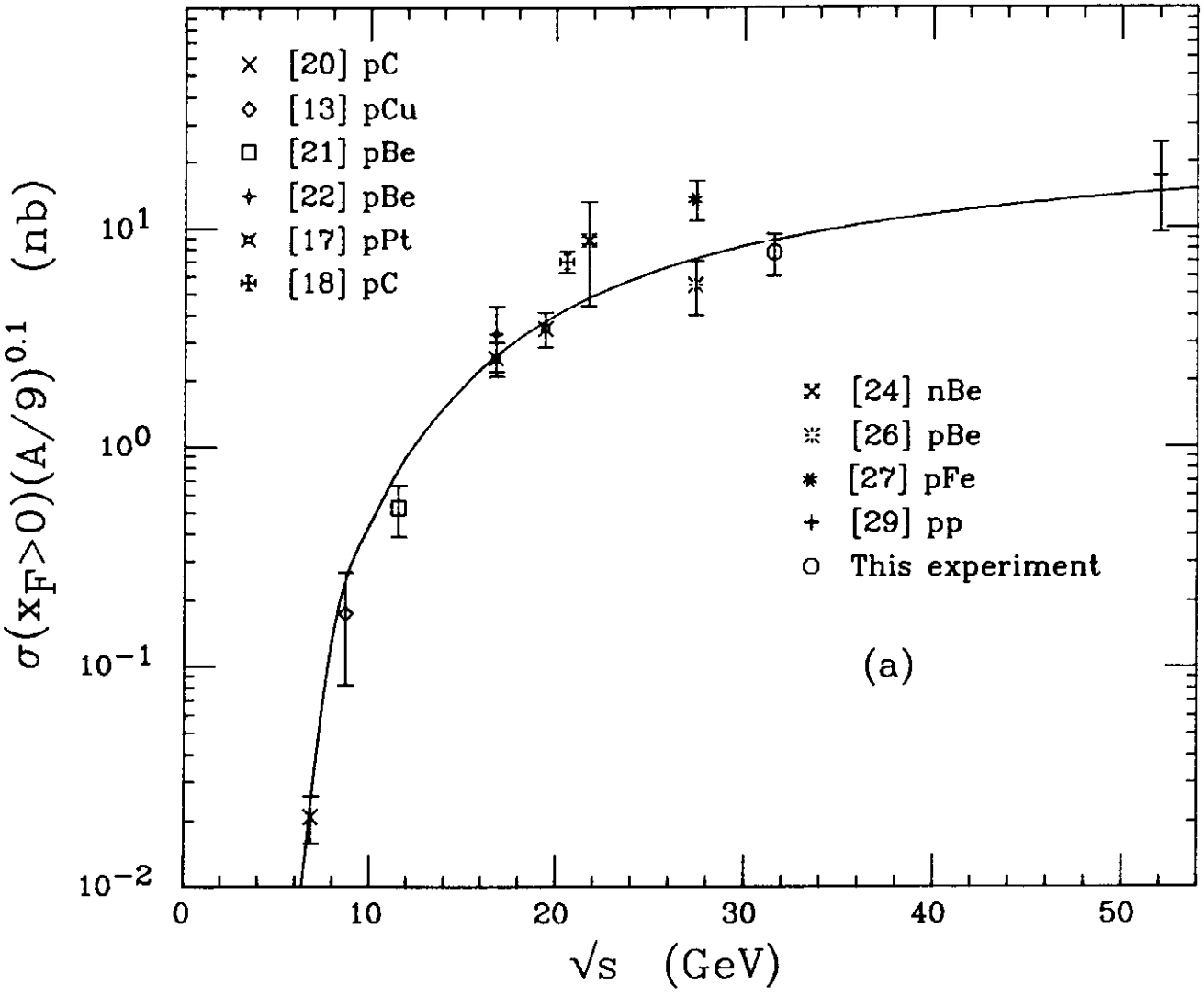
[20] pC
[13] pCu
[21] pBe
[22] pBe
[17] pPt
[18] pC
[24] nBe
[26] pBe
[27] pFe
[29] pp
This experiment
(a)
$\sigma(x_F>0)(A/9)^{0.1}$ (nb)
10^1
10^0
10^{-1}
10^{-2}
0
10
20
30
40
50
$\sqrt{s}$ (GeV)

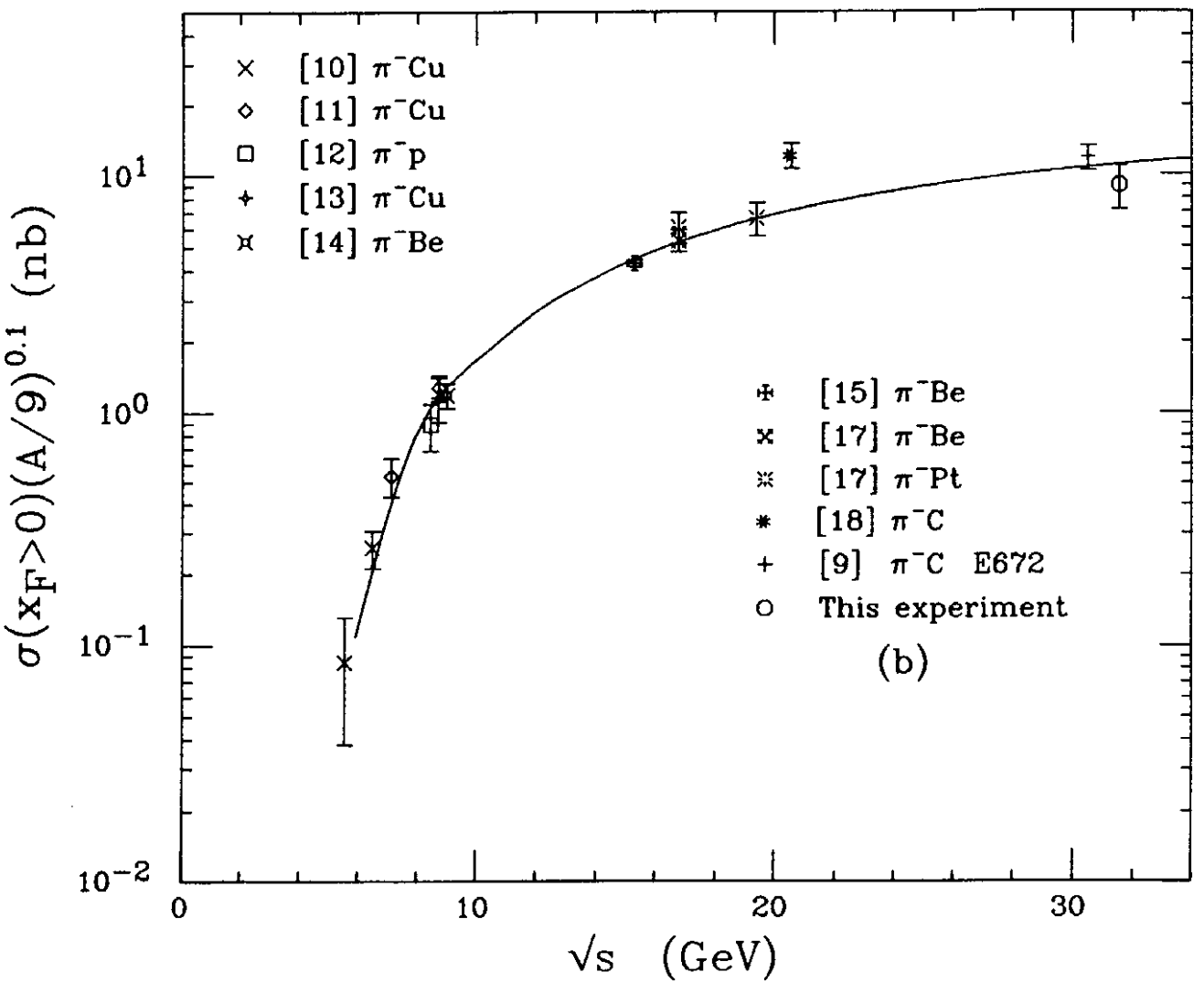
[10] π⁻Cu
[11] π⁻Cu
[12] π⁻p
[13] π⁻Cu
[14] π⁻Be
[15] π⁻Be
[17] π⁻Be
[17] π⁻Pt
[18] π⁻C
[9] π⁻C E672
This experiment
(b)
σ(x_F>0)(A/9)^0.1 (nb)
√s (GeV)
10^1
10^0
10^-1
10^-2
0
10
20
30

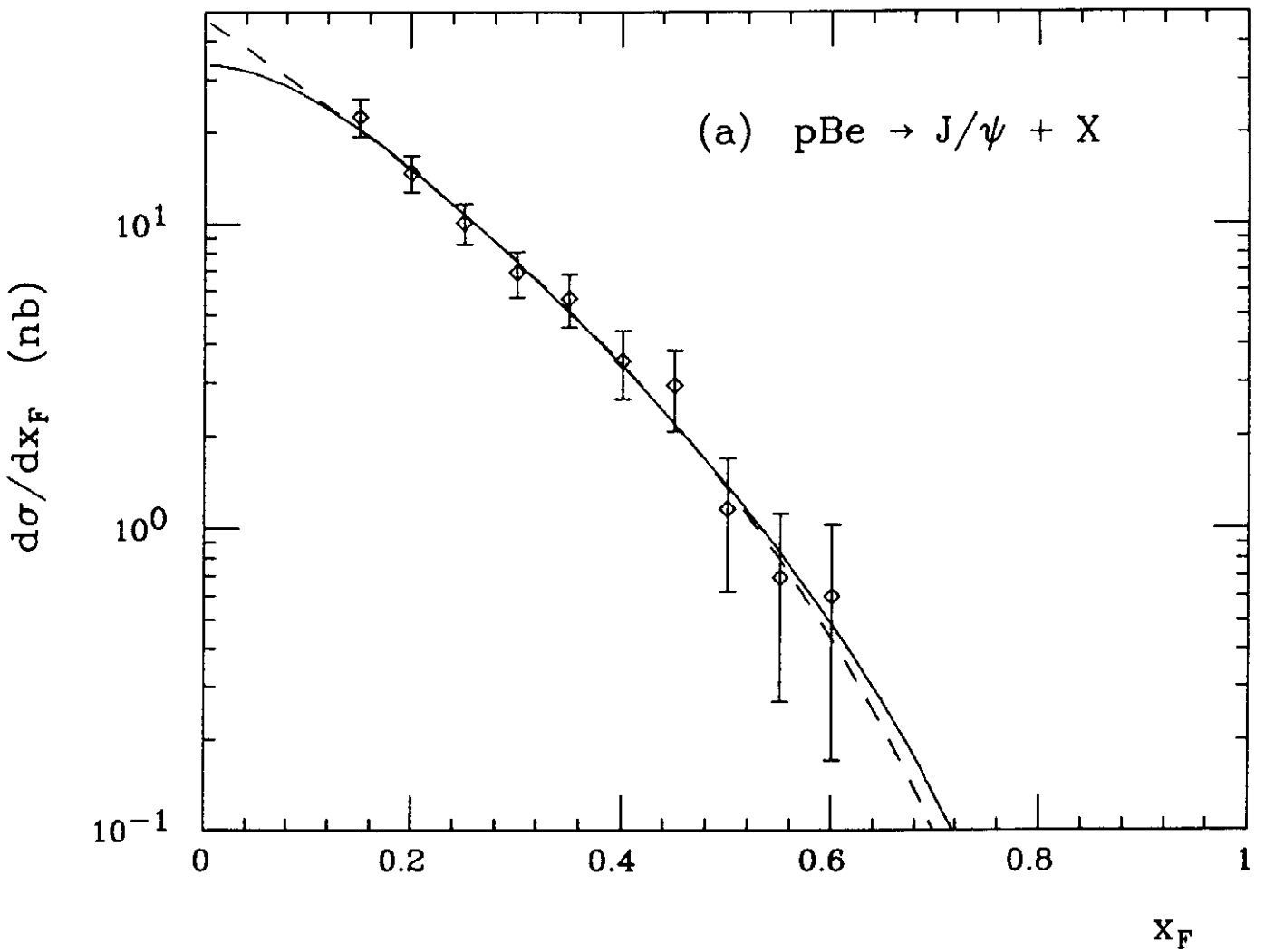
(a) pBe → J/ψ + X
dσ/dx_F (nb)
10^1
10^0
10^-1
0
0.2
0.4
0.6
0.8
1
x_F

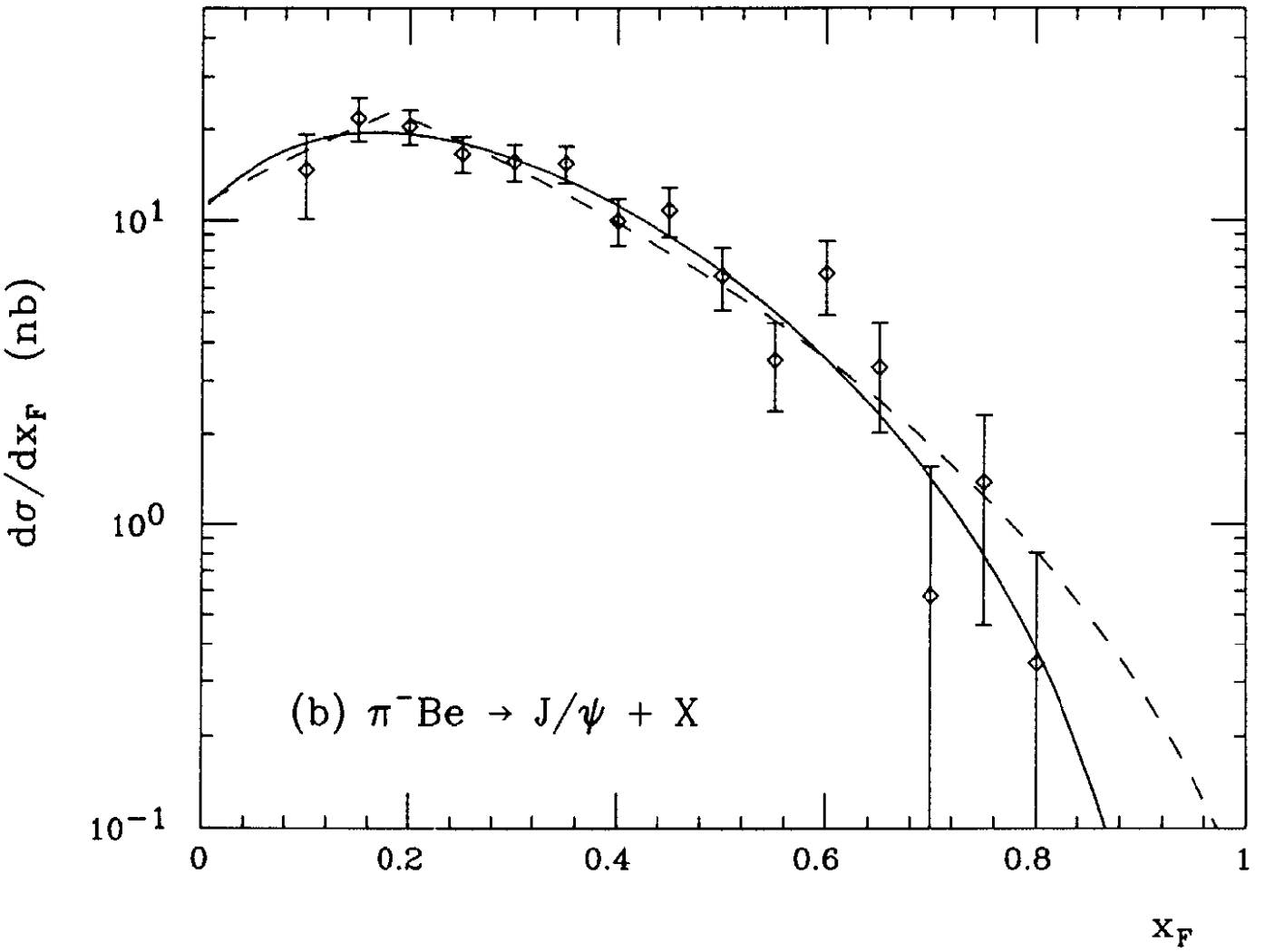
$d\sigma/dx_F$ (nb)
10^1
10^0
10^{-1}
0
0.2
0.4
0.6
0.8
1
x_F
(b) π^-Be $\rightarrow$ J/ψ + X

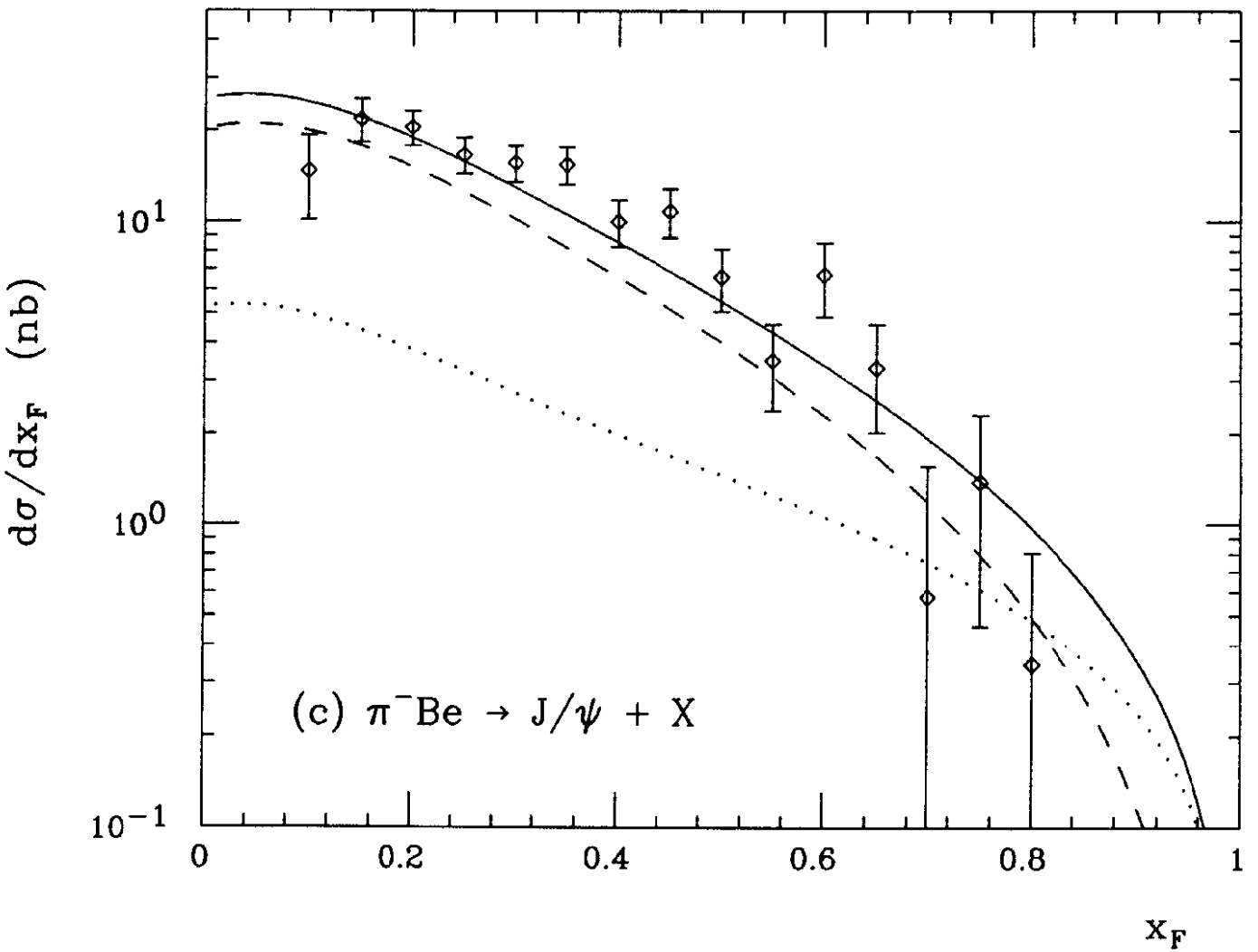
$d\sigma/dx_F$ (nb)
10^1
10^0
10^{-1}
0
0.2
0.4
0.6
0.8
1
x_F
(c) π^-Be → J/ψ + X

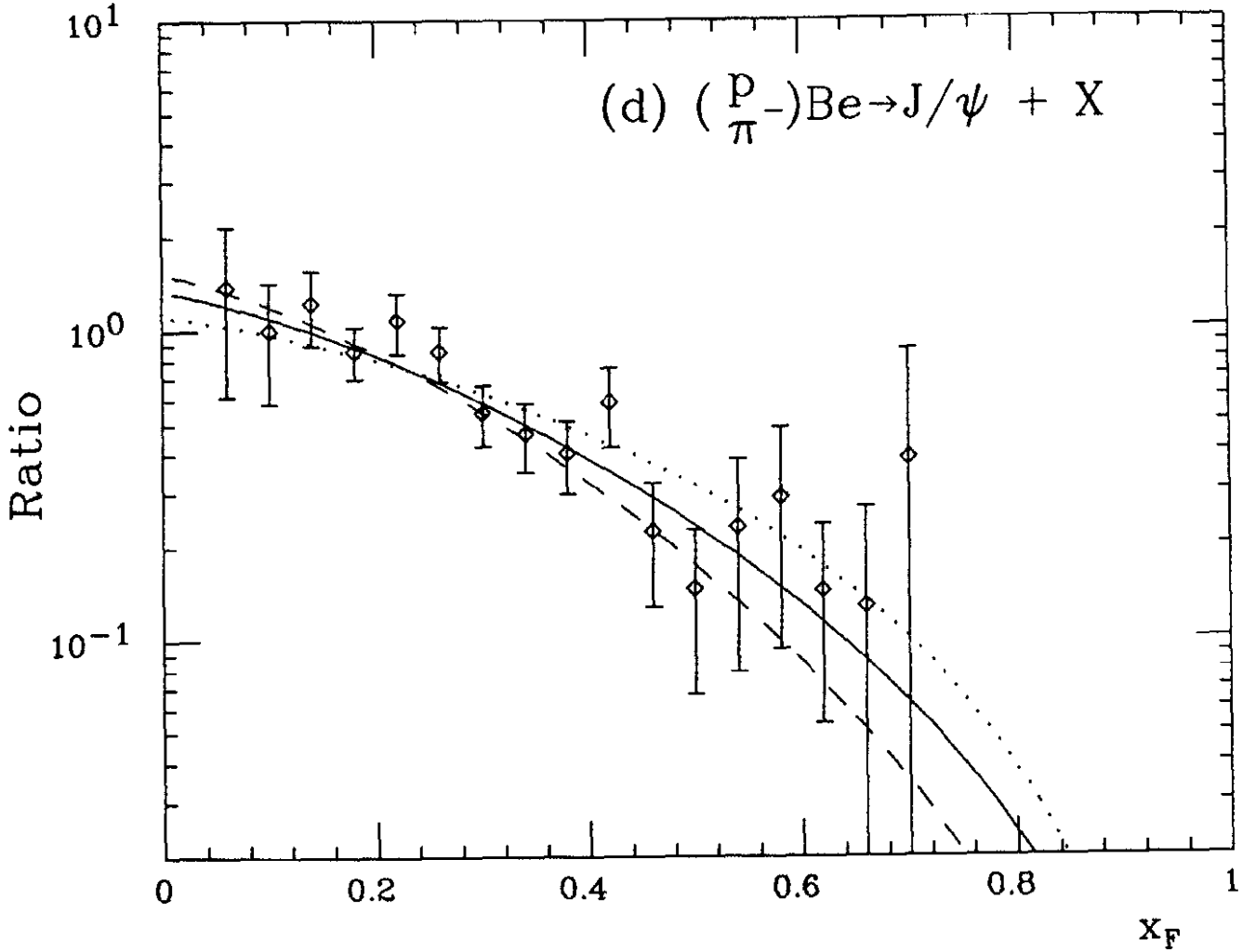
(d) (p/π-)Be→J/ψ + X
Ratio
10^1
10^0
10^-1
0
0.2
0.4
0.6
0.8
1
x_F

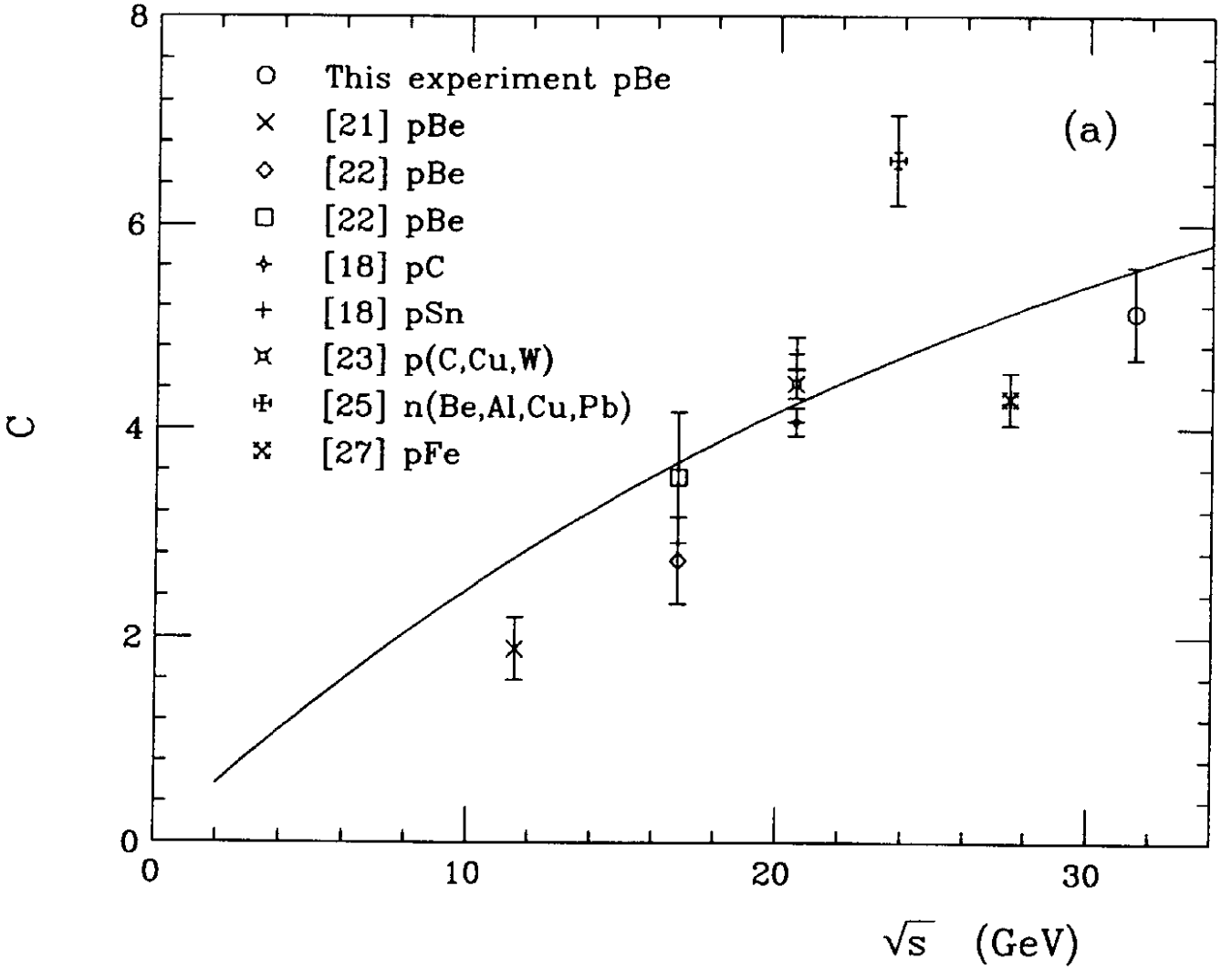
This experiment pBe
[21] pBe
[22] pBe
[22] pBe
[18] pC
[18] pSn
[23] p(C,Cu,W)
[25] n(Be,Al,Cu,Pb)
[27] pFe
(a)
C
0
2
4
6
8
0
10
20
30
√s (GeV)

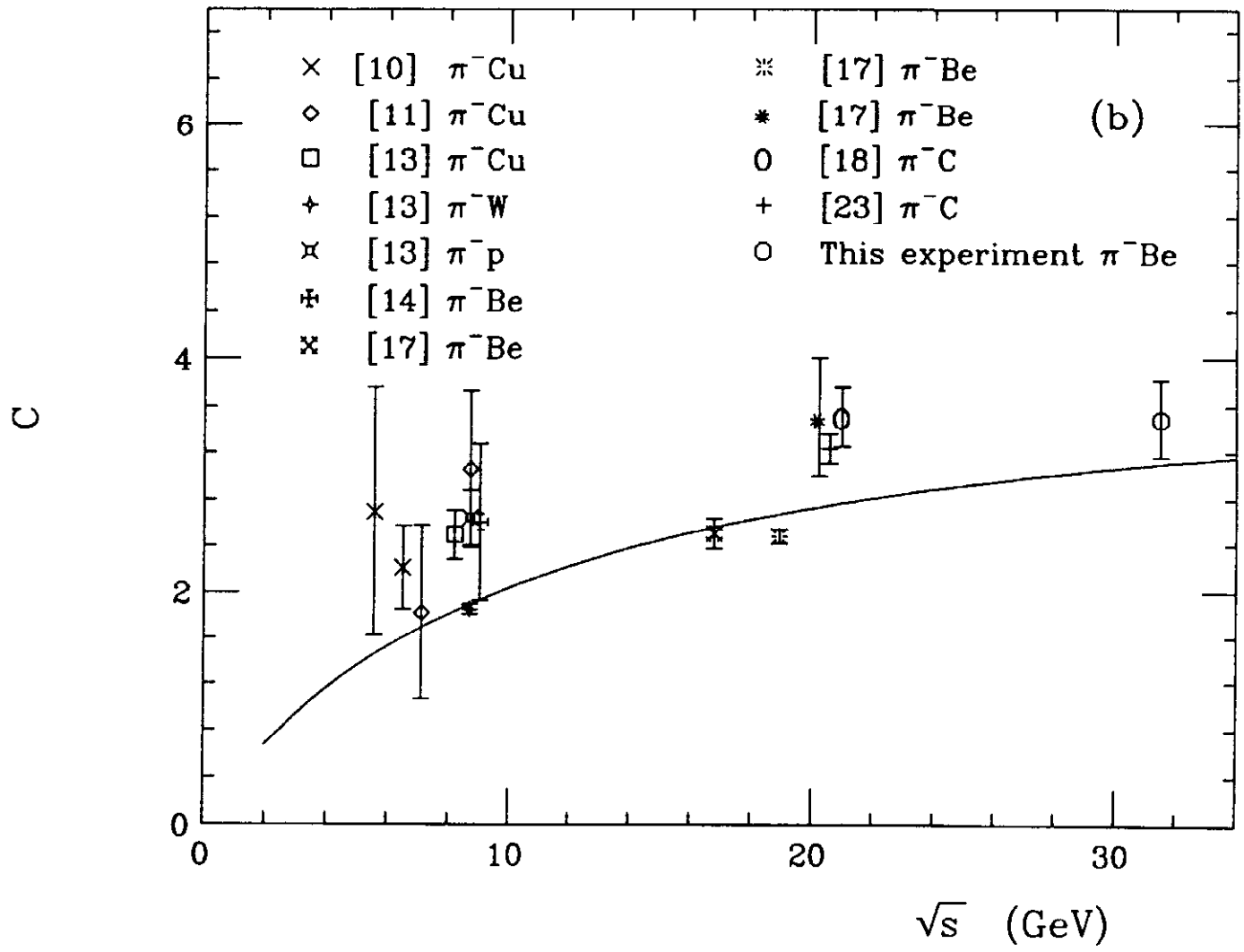
[10] π⁻Cu
[11] π⁻Cu
[13] π⁻Cu
[13] π⁻W
[13] π⁻p
[14] π⁻Be
[17] π⁻Be
[17] π⁻Be
[17] π⁻Be
[18] π⁻C
[23] π⁻C
This experiment π⁻Be
(b)
C
0
2
4
6
0
10
20
30
√s (GeV)

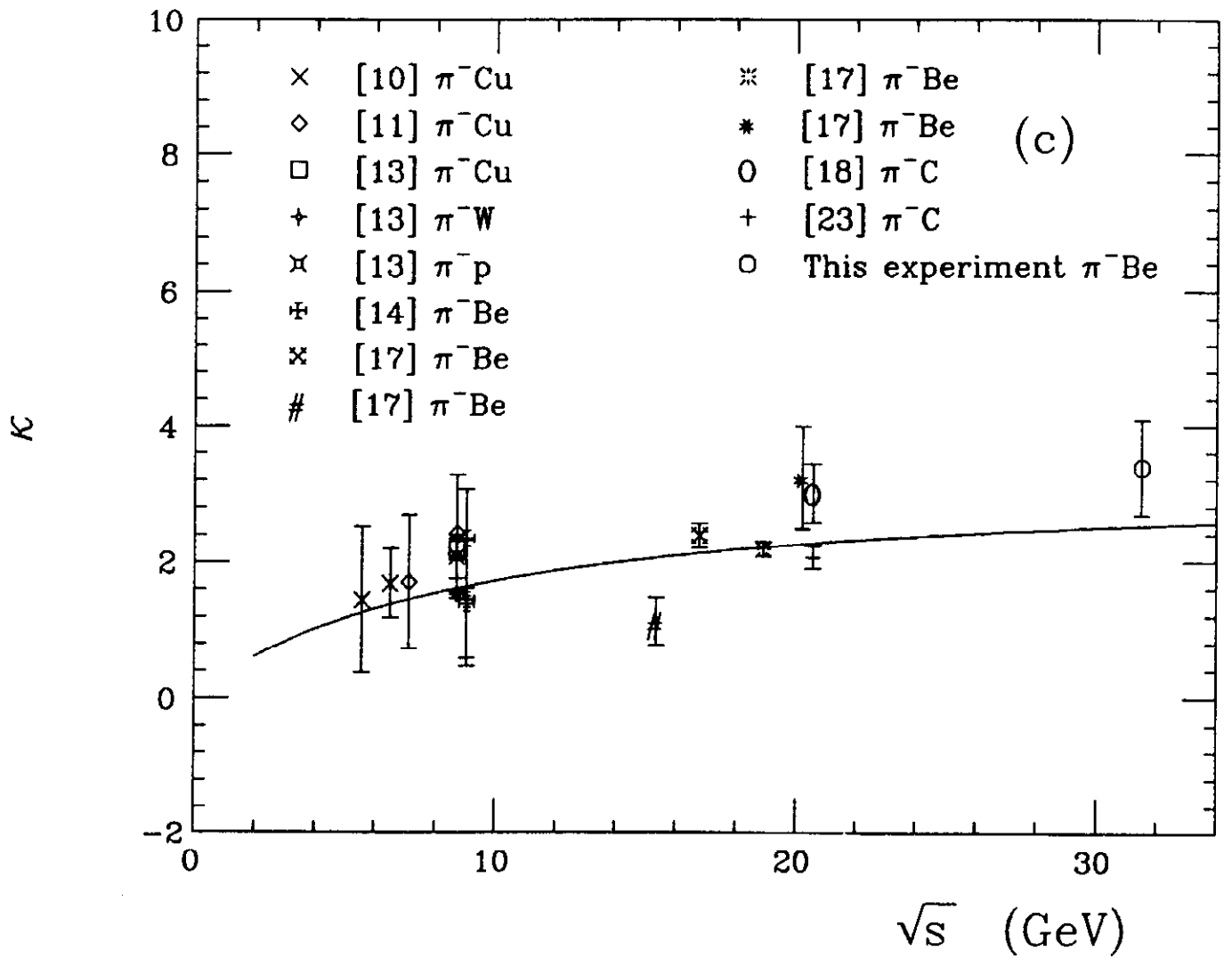
10
8
6
4
2
0
−2
0
10
20
30
$\mathcal{K}$
$\sqrt{s}$ (GeV)
× [10] π⁻Cu
◇ [11] π⁻Cu
□ [13] π⁻Cu
✦ [13] π⁻W
⌑ [13] π⁻p
⊕ [14] π⁻Be
⋇ [17] π⁻Be
[17] π⁻Be
⋇ [17] π⁻Be
* [17] π⁻Be
O [18] π⁻C
+ [23] π⁻C
O This experiment π⁻Be
(c)

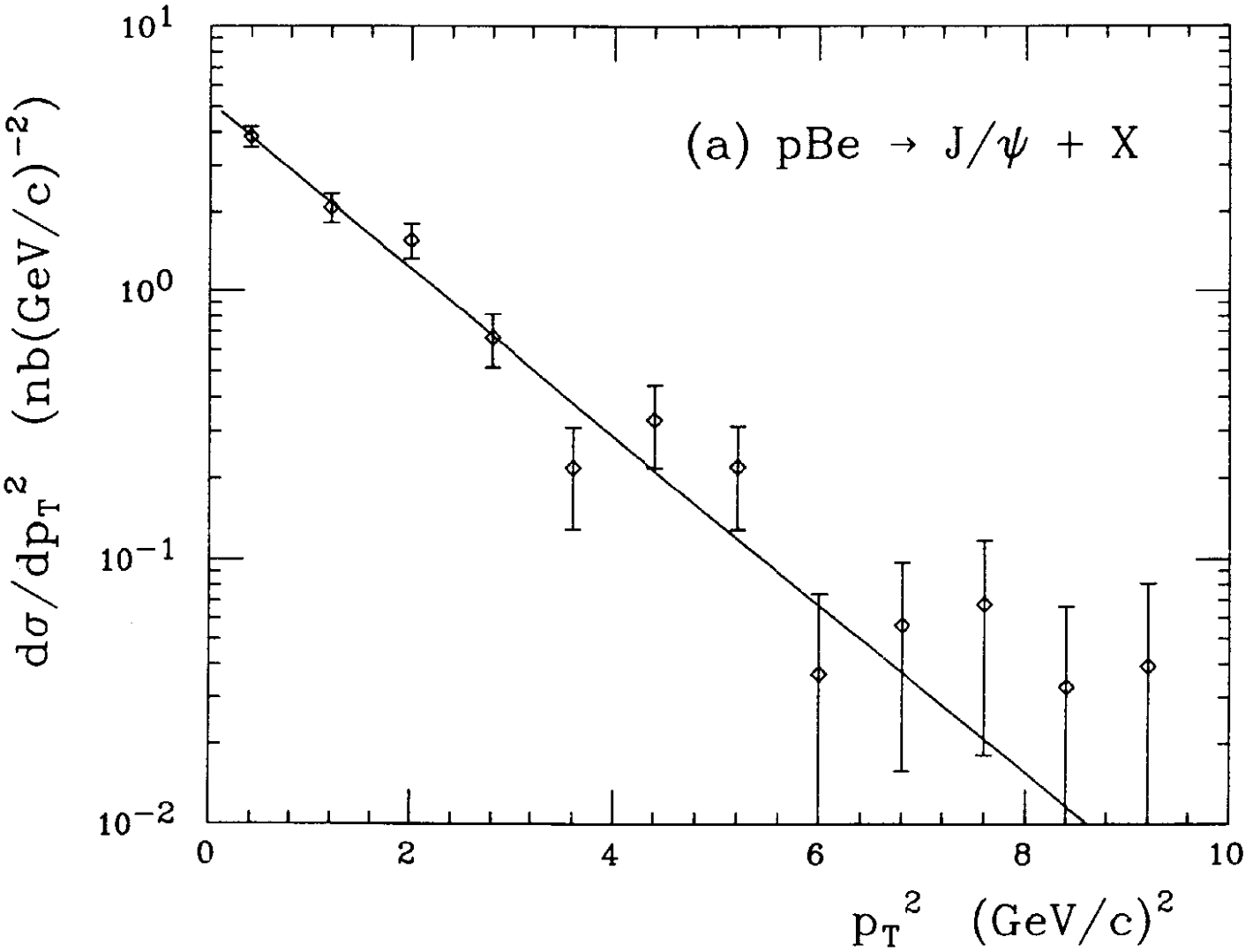
(a) pBe → J/ψ + X
dσ/dp_T^2 (nb(GeV/c)^-2)
p_T^2 (GeV/c)^2
10^1
10^0
10^-1
10^-2
0
2
4
6
8
10

August 20, 1990 V.Abramov et al., Fig. 8b.

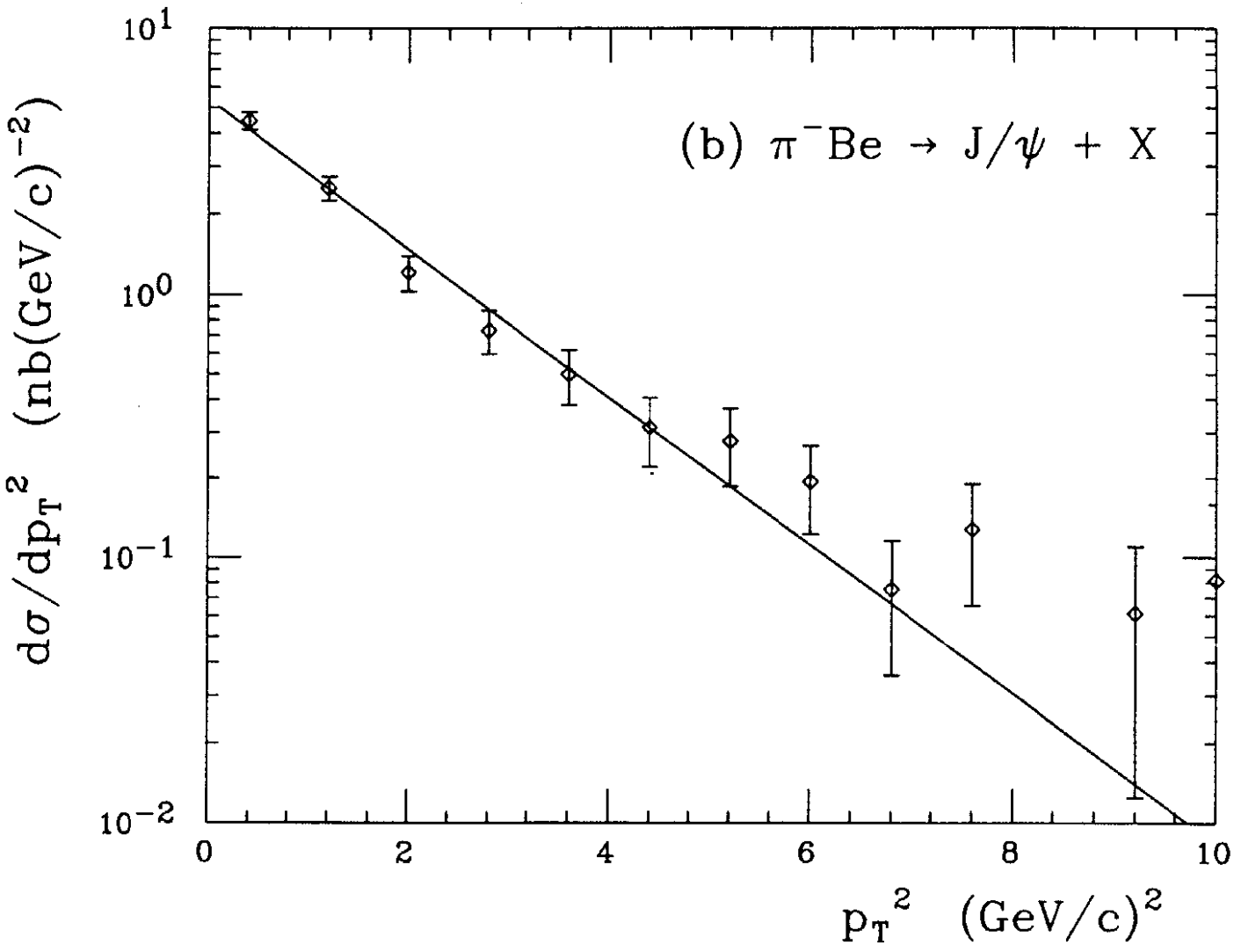

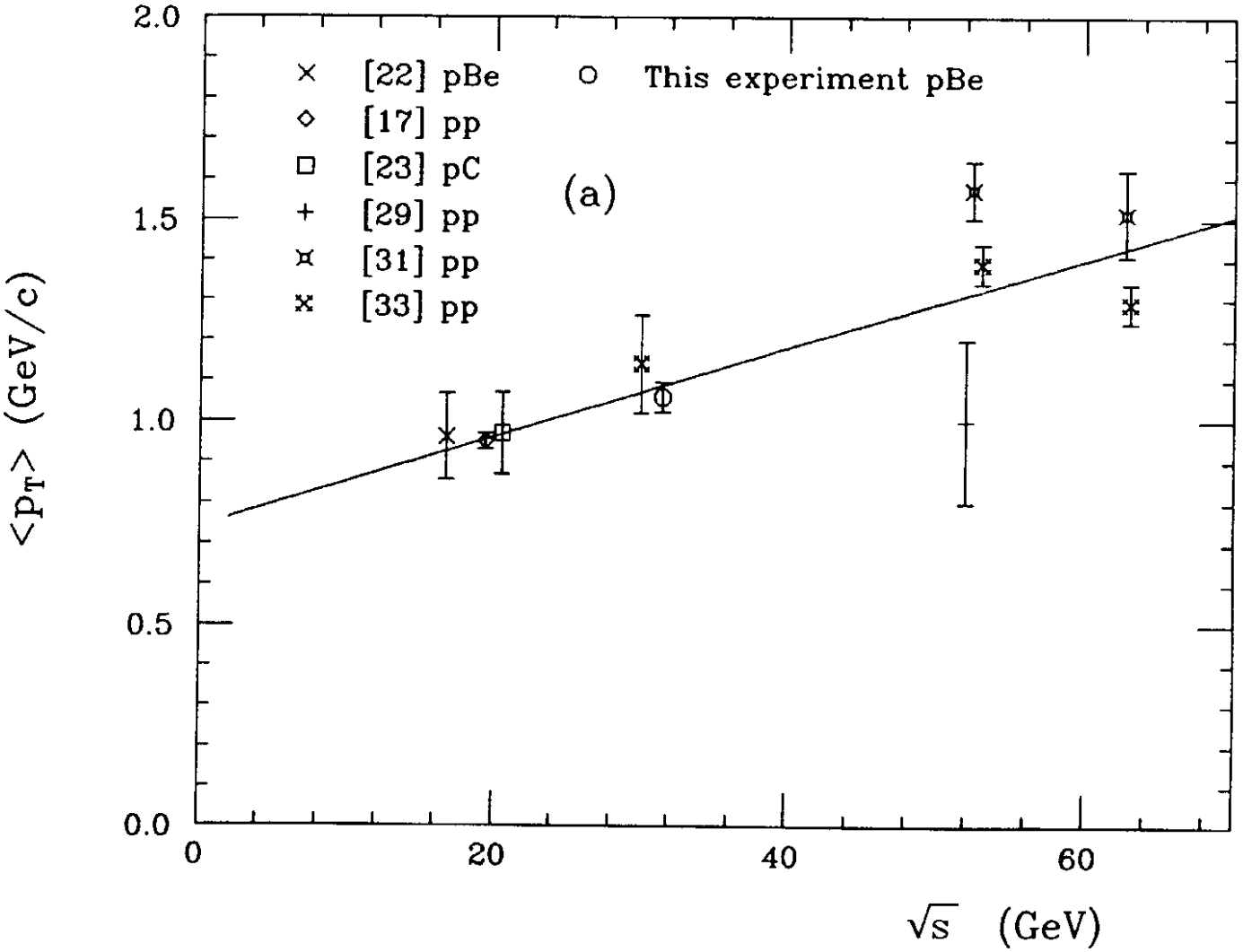
2.0
1.5
1.0
0.5
0.0
0
20
40
60
$\langle p_T \rangle$ (GeV/c)
$\sqrt{s}$ (GeV)
[22] pBe
This experiment pBe
[17] pp
[23] pC
[29] pp
[31] pp
[33] pp
(a)

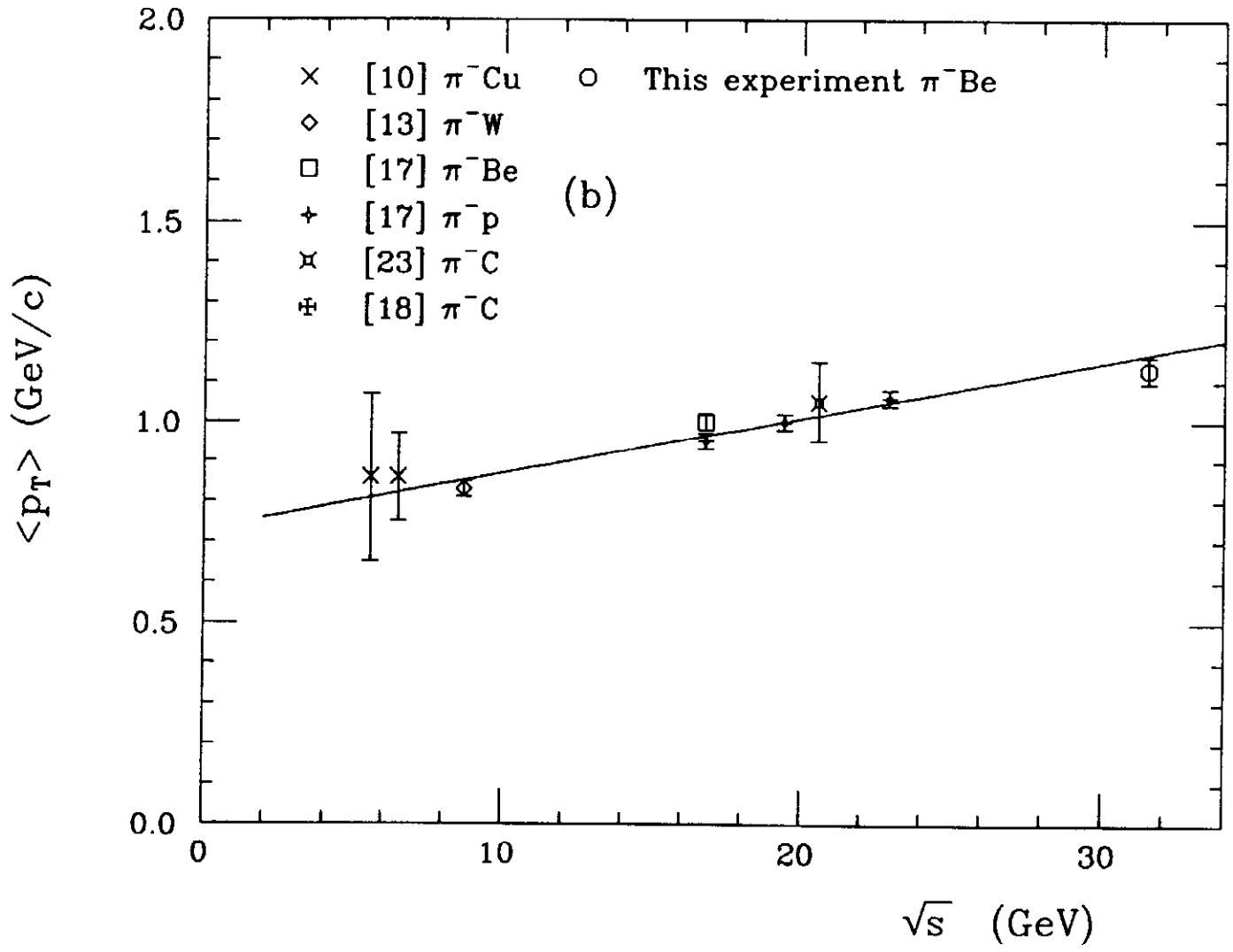
2.0
1.5
1.0
0.5
0.0
0
10
20
30
$\sqrt{s}$ (GeV)
$\langle p_T \rangle$ (GeV/c)
[10] π^-Cu
This experiment π^-Be
[13] π^-W
[17] π^-Be
[17] π^-p
[23] π^-C
[18] π^-C
(b)

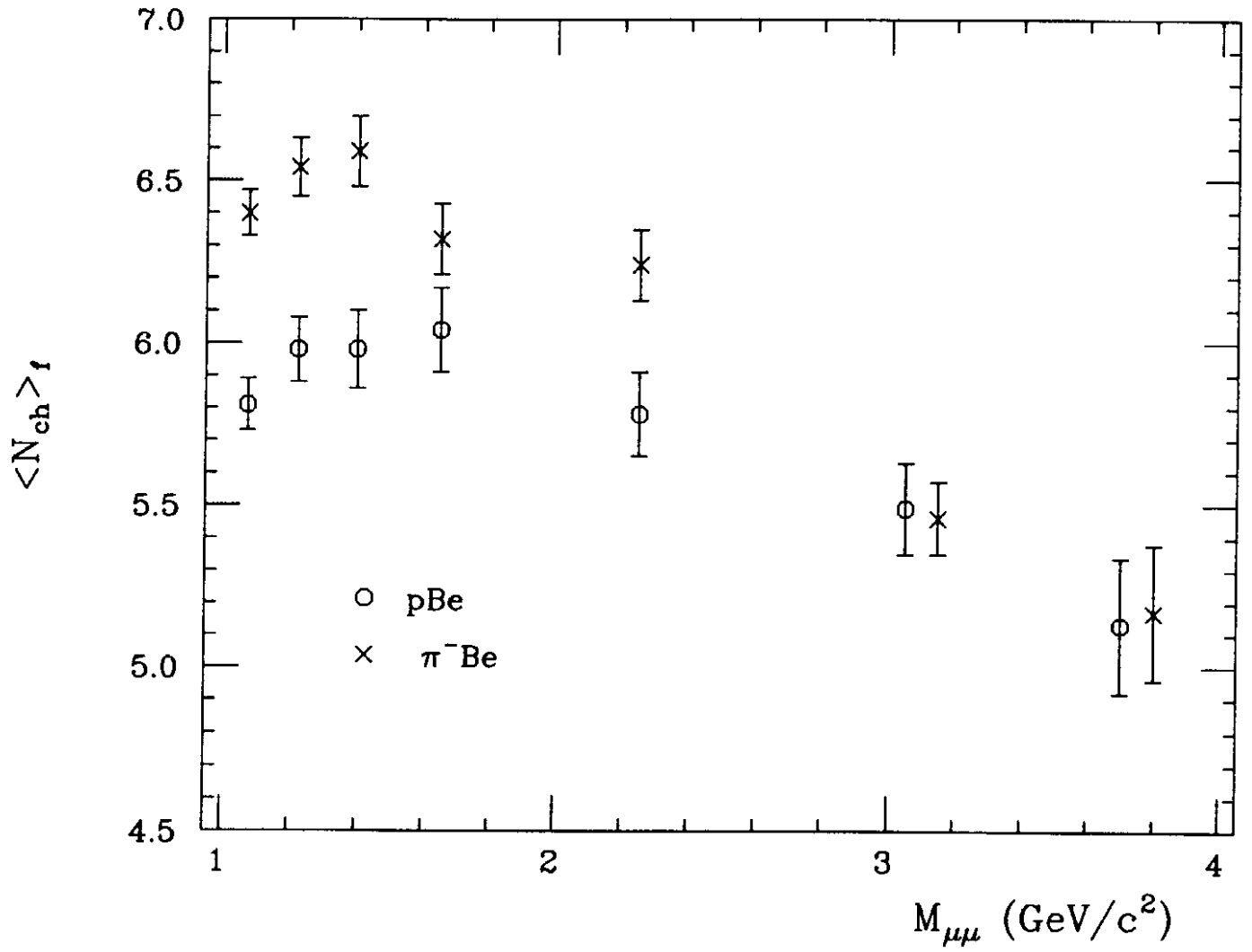
7.0
6.5
6.0
5.5
5.0
4.5
1
2
3
4
$\langle N_{ch} \rangle_t$
pBe
π^-Be
$M_{\mu\mu}$ (GeV/c^2)

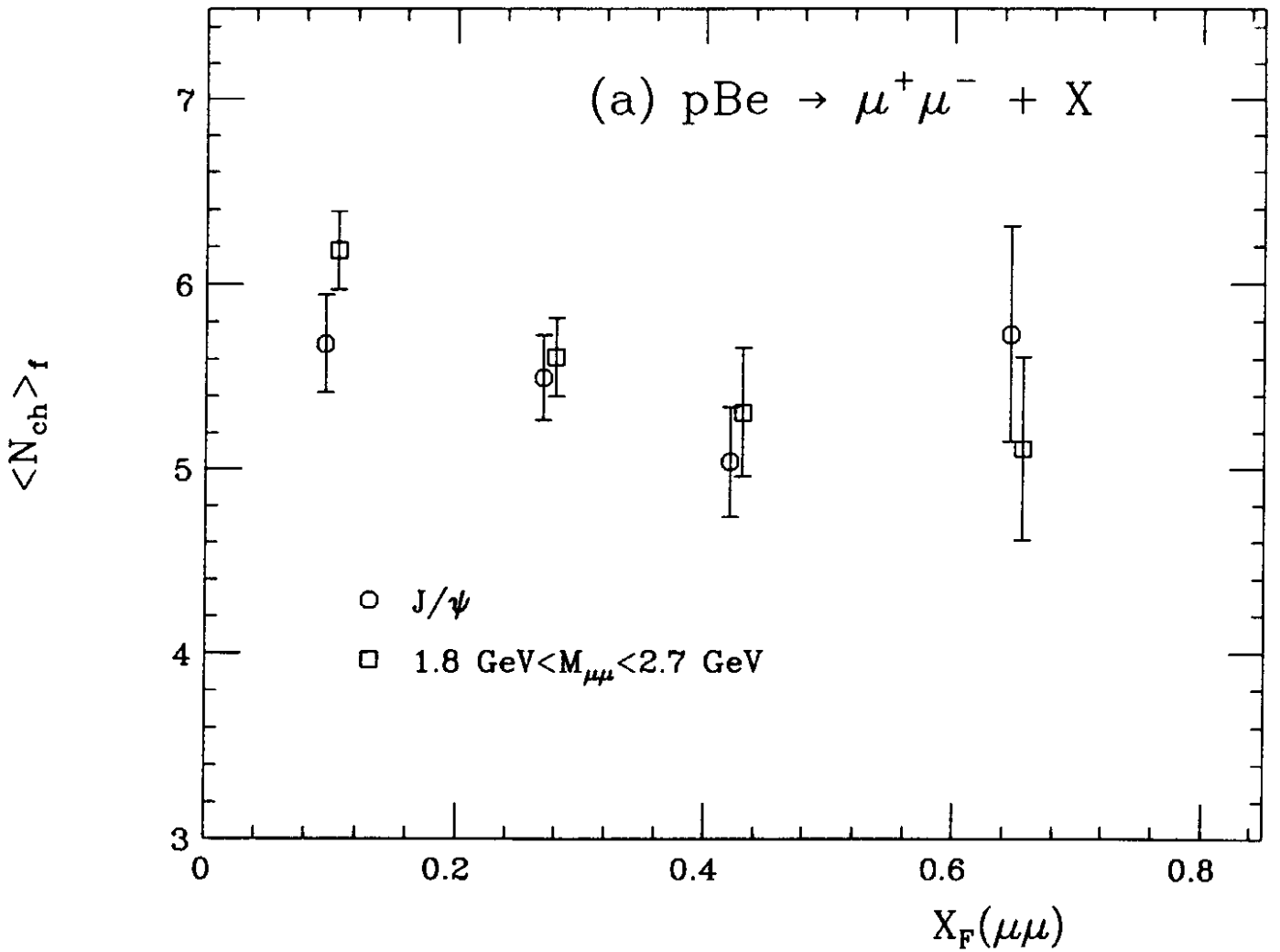
(a) pBe → $\mu^+\mu^-$ + X
$<N_{ch}>_f$
$X_F(\mu\mu)$
J/ψ
1.8 GeV<$M_{\mu\mu}$<2.7 GeV
7
6
5
4
3
0
0.2
0.4
0.6
0.8

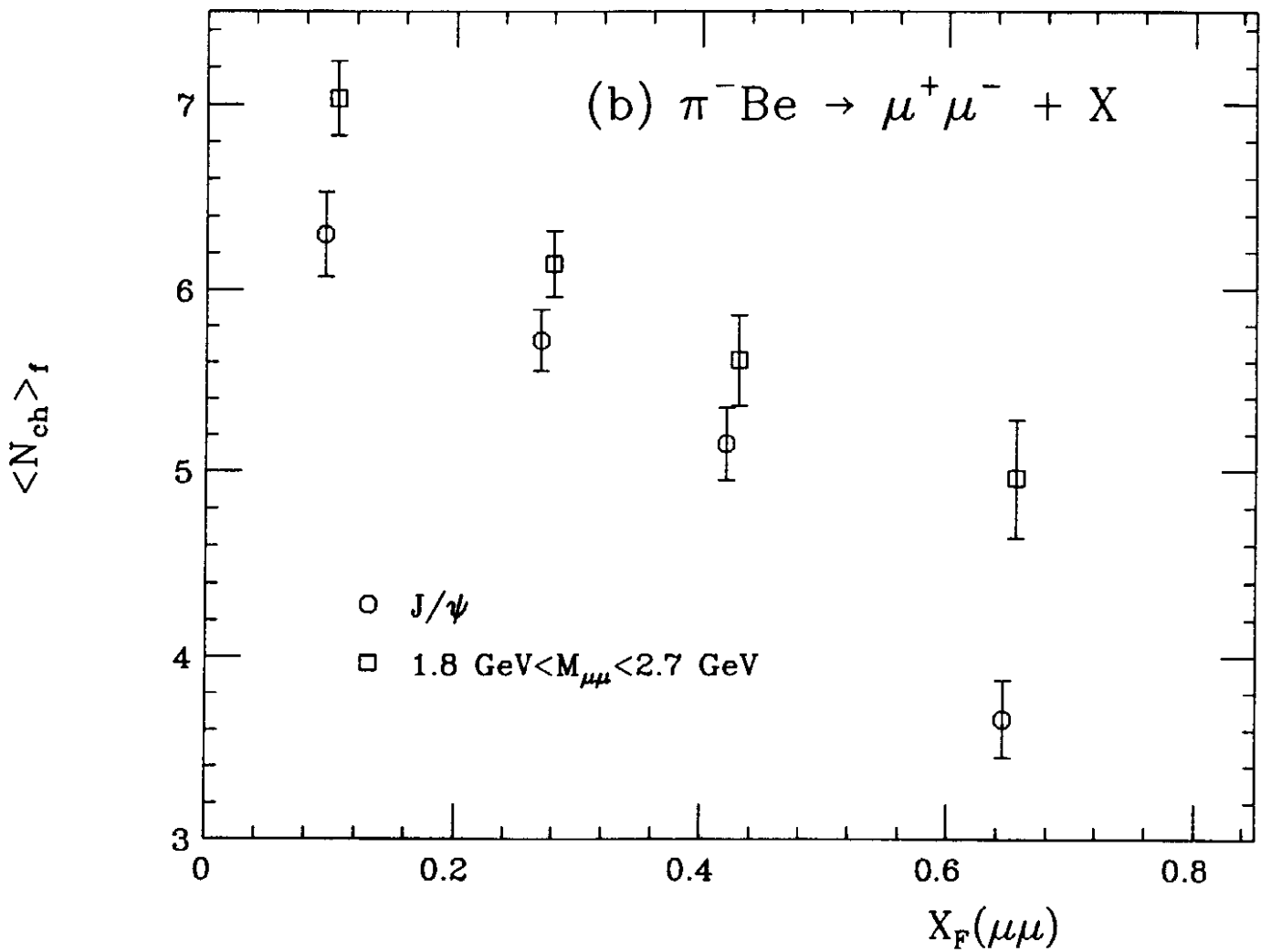
(b) $\pi^- Be \rightarrow \mu^+\mu^- + X$
$\langle N_{ch} \rangle_f$
$X_F(\mu\mu)$
J/ψ
1.8 GeV<M$_{\mu\mu}$<2.7 GeV
7
6
5
4
3
0
0.2
0.4
0.6
0.8

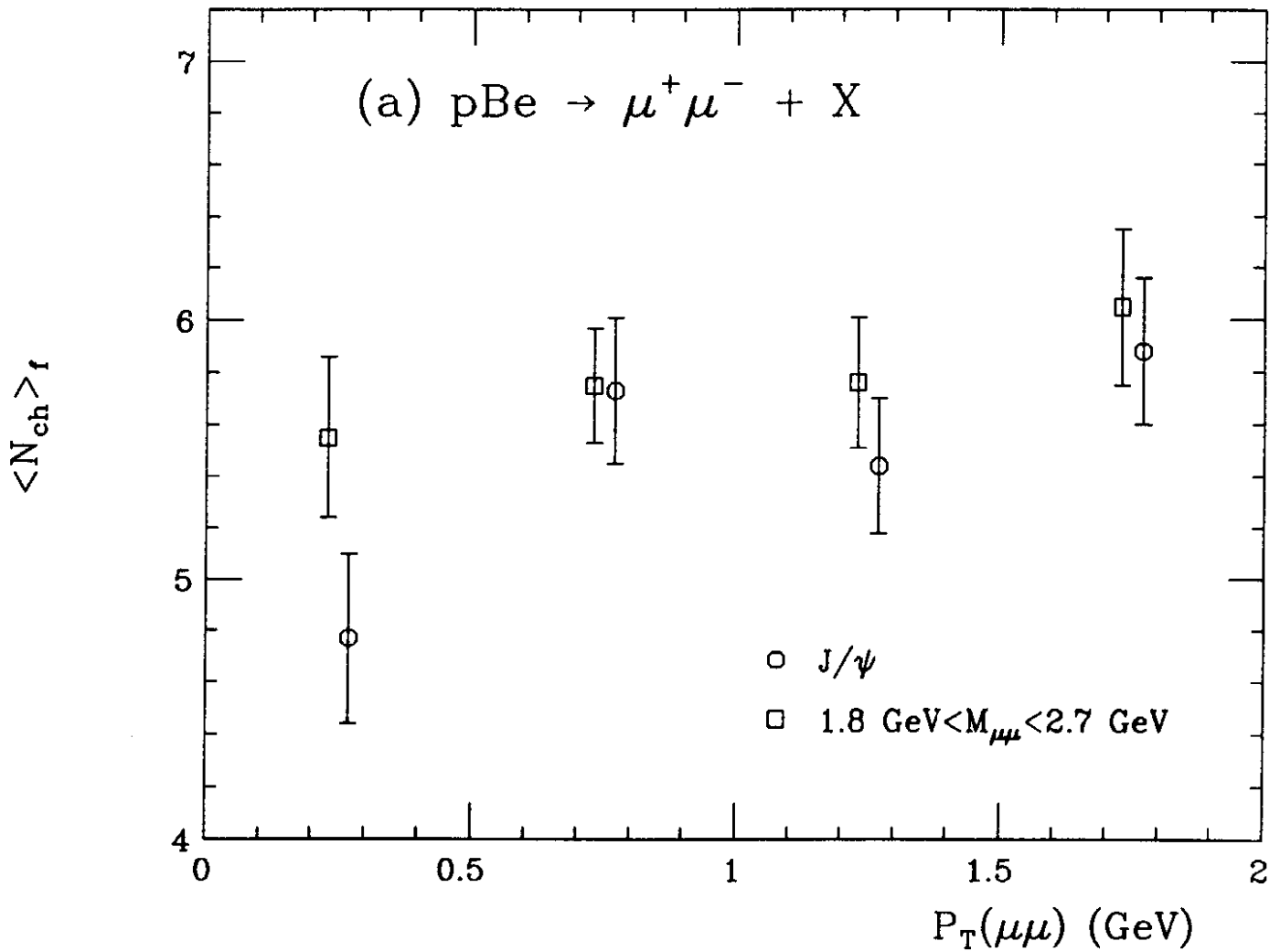
(a) pBe → $\mu^+\mu^-$ + X
$<N_{ch}>_f$
7
6
5
4
0
0.5
1
1.5
2
$P_T(\mu\mu)$ (GeV)
J/ψ
1.8 GeV<$M_{\mu\mu}$<2.7 GeV

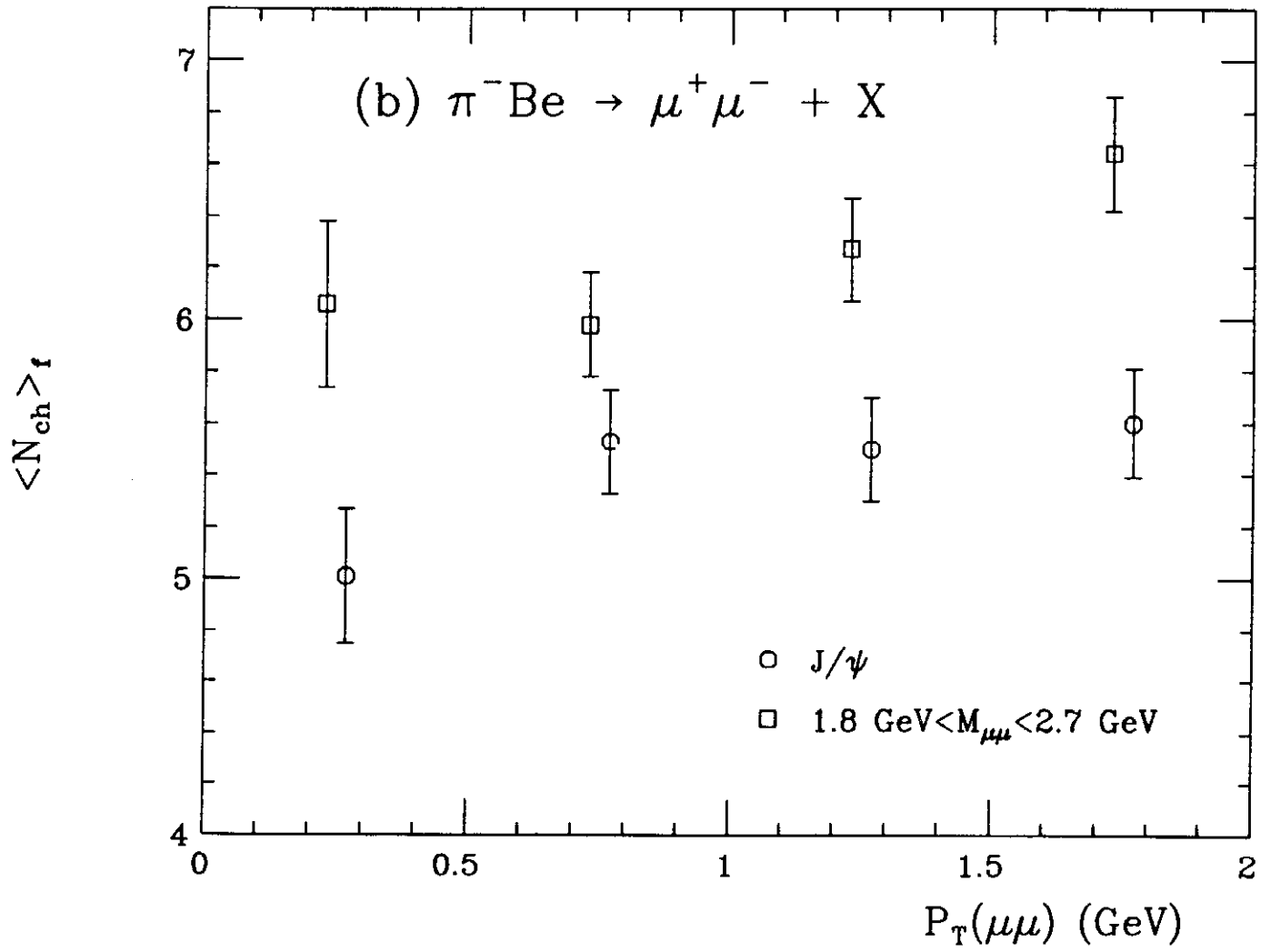
(b) π^-Be $\rightarrow \mu^+\mu^-$ + X
$<N_{ch}>_f$
7
6
5
4
0
0.5
1
1.5
2
$P_T(\mu\mu)$ (GeV)
J/ψ
1.8 GeV<$M_{\mu\mu}$<2.7 GeV

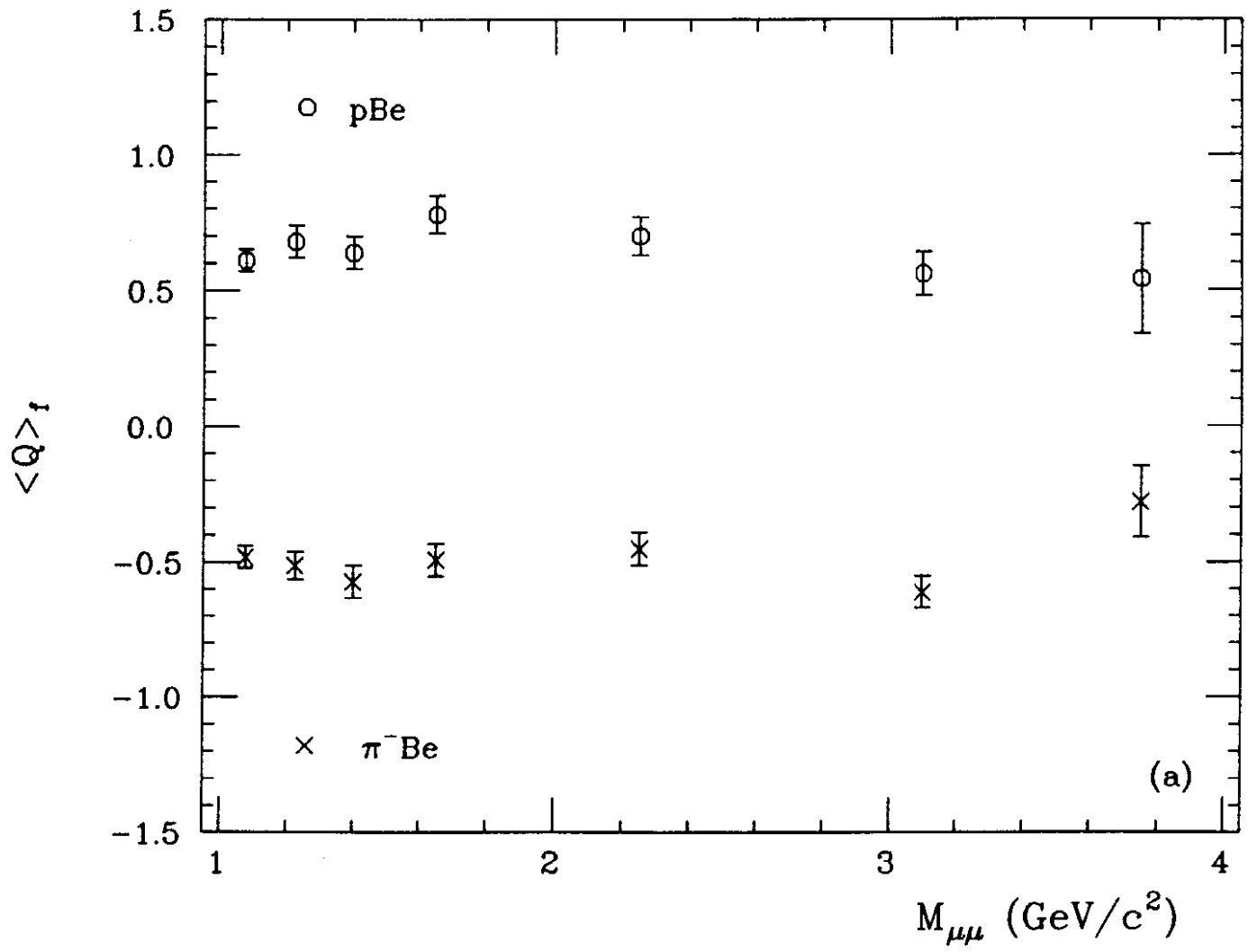
1.5
1.0
0.5
0.0
−0.5
−1.0
−1.5
1
2
3
4
pBe
π⁻Be
(a)
<Q>f
Mμμ (GeV/c²)

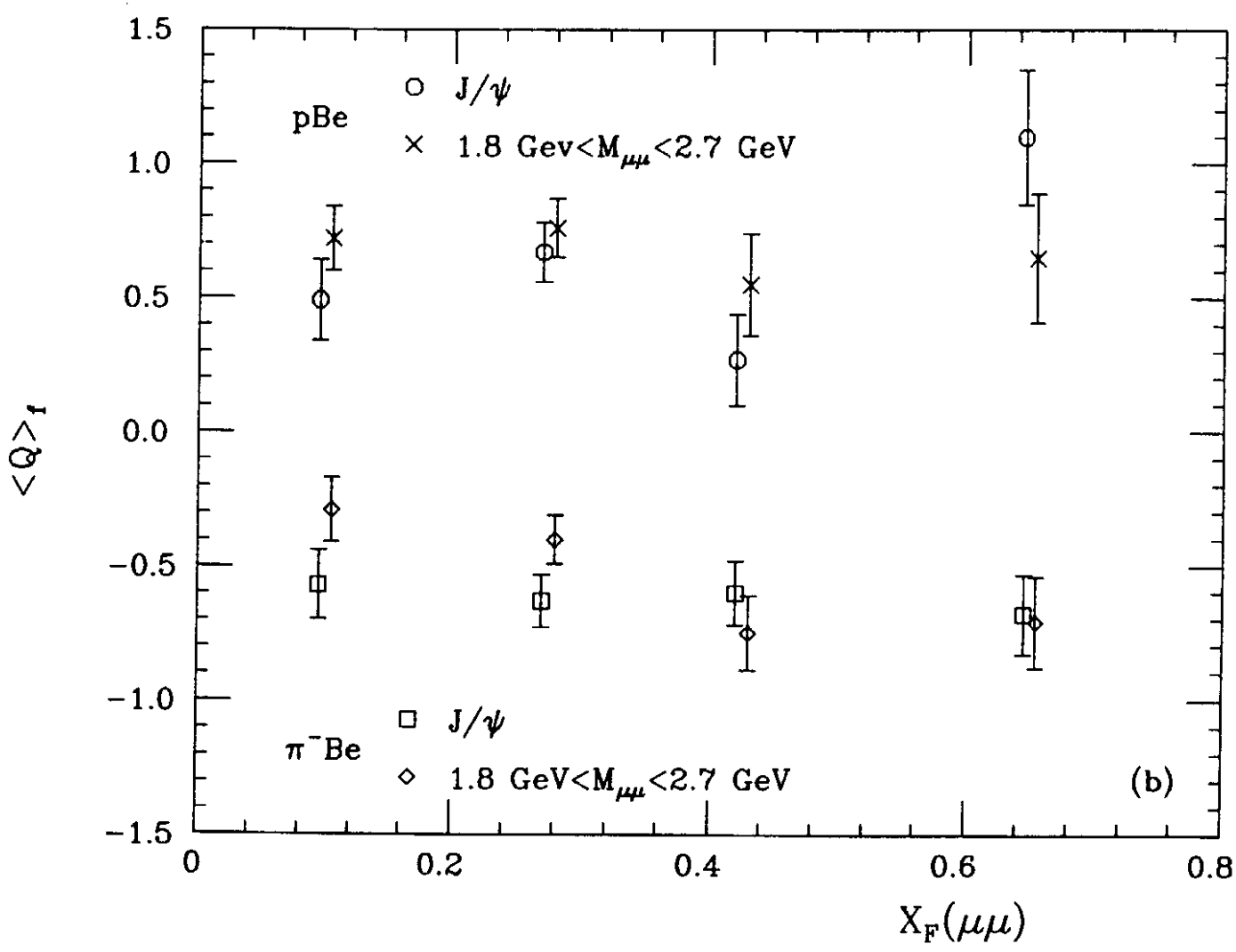
1.5
1.0
0.5
0.0
−0.5
−1.0
−1.5
0
0.2
0.4
0.6
0.8
$\langle Q \rangle_f$
$X_F(\mu\mu)$
pBe
J/ψ
1.8 Gev<M$_{\mu\mu}$<2.7 GeV
π⁻Be
J/ψ
1.8 GeV<M$_{\mu\mu}$<2.7 GeV
(b)

V.Abramov et al., Fig. 13.c

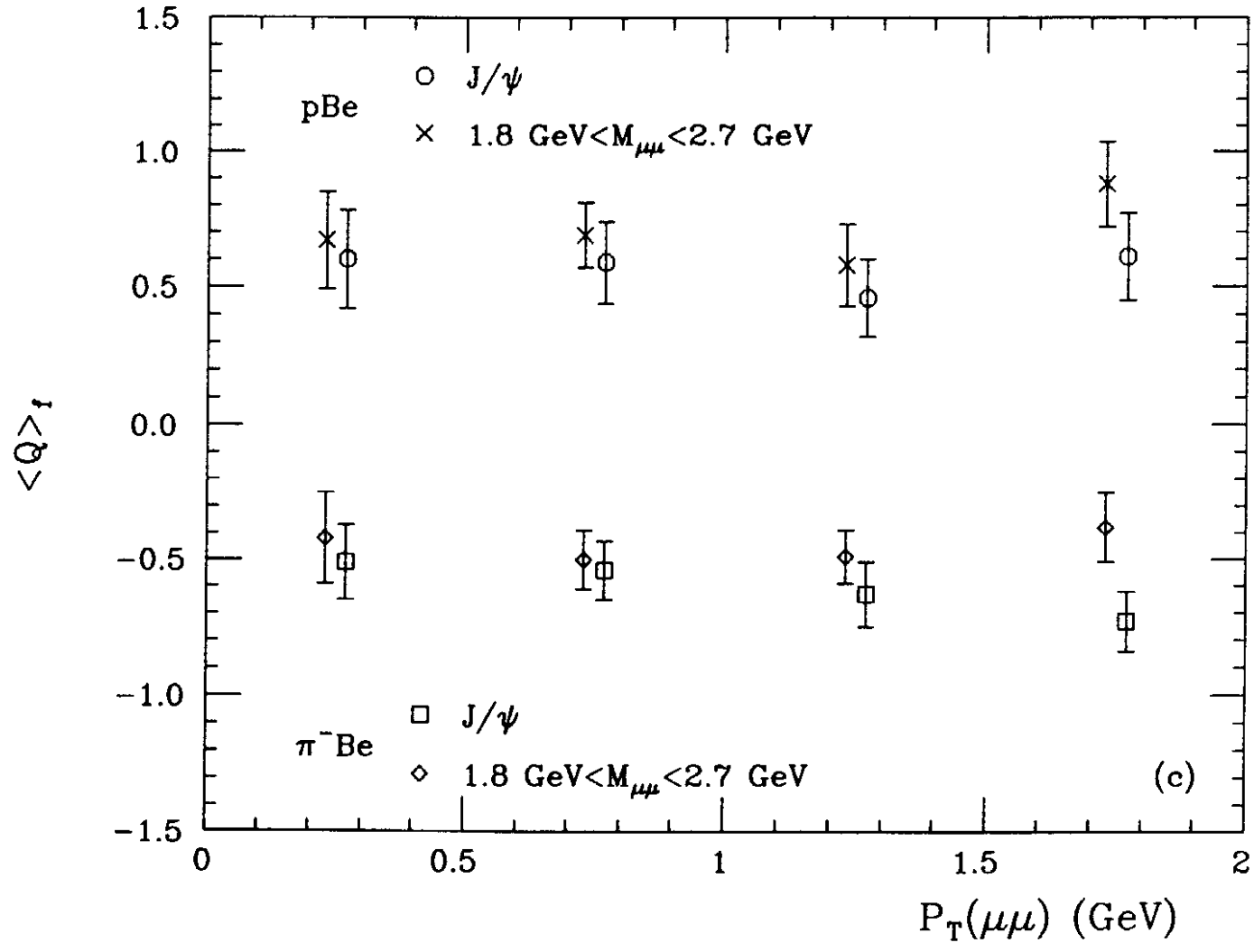

V.Abramov et al., Fig. 14.